UPPSALA
UNIVERSITET

Digital Comprehensive Summaries of Uppsala Dissertations from the Faculty of Science and Technology 1666

Opportunities and challenges of surface scattering at next generation neutron sources

FRANZ ALOIS ADLMANN

ACTA
UNIVERSITATIS
UPSALIENSIS
UPPSALA
2018

ISSN 1651-6214
ISBN 978-91-513-0324-6
urn:nbn:se:uu:diva-348348

Dissertation presented at Uppsala University to be publicly examined in Häggsalen, Ångströmlaboratoriet, Lägerhyddsvägen 1, Uppsala, Friday, 25 May 2018 at 13:30 for the degree of Doctor of Philosophy. The examination will be conducted in English. Faculty examiner: Dr Henrich Frielinghaus (Jülich Centre for Neutron Science JCNS at Heinz Maier-Leibnitz Zentrum (MLZ), Munich, Germany).

Abstract
Adlmann, F. A. 2018. Opportunities and challenges of surface scattering at next generation neutron sources. *Digital Comprehensive Summaries of Uppsala Dissertations from the Faculty of Science and Technology* 1666. 51 pp. Uppsala: Acta Universitatis Upsaliensis. ISBN 978-91-513-0324-6.

Complex fluids and soft matter are ubiquitously found in the world and all contacts in life are made over surfaces. To describe the mechanical behavior of such substances, rheological methods are used. Flow instabilities are a big challenge in rheology since they will be reflected in the macroscopic variables probed, like e. g. the viscosity. Many such discontinuities may actually originate at the surface. Investigating the properties of liquids in contact with the surface under mechanical load is the main course of the thesis. Neutron reflectometry and GISANS are perfect tools in this context to access the solid liquid interfaces, since they can penetrate many engineering materials and show a comparably large scattering potential at deuterated samples. In this thesis shear was applied on a model solution and neutron scattering techniques were used to investigate the structure under load. The focus was set on the development of the measurement methods themselves to enable new scientific insights in the future. First, by stroboscopic measurements the flux limitations are overcome for oscillatory rheology. By reintegration in the post processing it is shown that kinetic measurements with neutrons are possible with a time resolution below one millisecond. Second, the transformation of grazing incidence data from the laboratory system into q-space is strongly non-linear resulting in a need for re-binning. In this thesis a universal tool has been developed for this purpose. Finally, there is an ongoing discussion on depth sensitive neutron scattering experiments from solid-liquid boundaries. By using emission densities we show that such experiments face severe limitations due to the low absorption cross section of the neutron.

Keywords: GISANS, data reduction, off-specular, neutron scattering, reflectometry, complex fluids, rheology

Franz Alois Adlmann, Department of Physics and Astronomy, Materials Physics, 516, Uppsala University, SE-751 20 Uppsala, Sweden.

ISSN 1651-6214
ISBN 978-91-513-0324-6
urn:nbn:se:uu:diva-348348 (http://urn.kb.se/resolve?urn=urn:nbn:se:uu:diva-348348)

"Yesterday's sensation is today's calibration."
R. P. Feynman
"...and tomorrow's background."
V. L. Telegdi.

Till min mor - Für meine Mutter

List of papers

This thesis is based on the following papers, which are referred to in the text by their Roman numerals.

I **Depth-resolved grazing-incidence time-of-flight neutron scattering from a solid liquid interface**
Wolff, M. ; Herbel, J. ; **Adlmann, F.** ; Dennison, A. J. C. ; Liesche, G. ; Gutfreund, P. and Rogers, S., *Journal of Applied Crystallography*, **47**, 100 (2014)

II **Towards neutron scattering experiments with sub-millisecond time resolution**
Adlmann, F. A. ; Gutfreund, P. ; Ankner, J. F. ; Browning, J. ; Parizzi, A. ; Vacaliuc, B. ; Halbert, C. E. ; Rich, J.P. ; Dennison, A. J. C. and Wolff, M. *Journal of Applied Crystallography*, **48**, 220 (2015)

III **Probing the dynamics of high-viscosity entangled polymers under shear using Neutron Spin Echo spectroscopy**
Kawecki, M. ; Gutfreund, P. ; **Adlmann, F. A.** ; Lindholm, E. ; Longeville, S. ; Lapp, A. ; Wolff, M. *Journal of Physics: Conference series*, **746**, 012014 (2016)

IV **'Överlåtaren': a fast way to transfer and orthogonalize two-dimensional off-specular reflectivity data**
Adlmann, F. A. ; Palsson, G. K. ; Bilheux, J. C. ; Ankner, J. F. ; Gutfreund, P. ; Kawecki, M. and Wolff, M., *Journal of Applied Crystallography*, **49**, 100 (2016)

V **Polymer Brush Collapse under Shear Flow**
Korolkovas, A. ; Rodriguez-Emmenegger , C. ; de los Santos Pereira, A. ; Chenneviere ,A. ; Restagno, F. ; Wolff, M. ; **Adlmann, F. A.**; Dennison, A. J. C. and Gutfreund, P. *Macromolecules*, **50**, 1215 (2017)

VI **Depth resolved grazing incidence neutron scattering experiments from semi-infinite interfaces: a statistical analysis of the scattering contributions**
Adlmann, F. A. ; Herbel, J. ; Korolkovas, A. ; Bliersbach, A. ; Toperverg, B. ; Van Herck, W.; Palsson, G. K.; Kitchen, B. and Wolff, M. *Journal of Physics: Condensed Matter*, **30**, 165901 (2018)

VII **Normalization and monitoring of stroboscopic neutron experiments**
Adlmann, F. A.; Vacaliuc, B. ; Ankner, J. F. ; Busch, S. ; Browning, J. F. ; Parizzi, A. ; Bilheux, J. F. ; and Wolff, M. *NIM B* (in manuscript)

Reprints were made with permission from the publishers.

My contributions to the papers in this thesis

I Participated heavily in the data treatment and co-supervised the sub-lining bachelor thesis.

II Designed the technique. Full responsibility for the software development, all measurements, the analysis and writing the manuscript.

III Partially responsibility for the rheology measurements. Co-supervised the sub-lining master's thesis. Participated in writing the paper.

IV Full responsibility for developing the algorithm, writing the GUI and writing the manuscript.

V Partizipated in the rheology measurements and contributed in the reflectivity measurements. Sample responsible for the whole project.

VI Performed the statistical analysis, designed the equations, wrote the corresponding code, performed the simulations and wrote the paper.

VII Full responsibility for developing the algorithm, performed the experiment and writing of the paper.

Contents

1. Introduction

> God made the bulk; surfaces were invented by the devil.
>
> Wolfgang Pauli

Plastics are ubiquitous in our modern world, since the possibilities of tuning their mechanical properties are literally infinite. This fact has led to an increased interest in polymer physics. One specific characteristic of polymers is that they may show both liquid and solid properties at the same time. Apparent examples from our everyday lives are rubber, tooth paste or plastic bags. All these materials feature the elastic properties of solids, however, if kept under constant load they will relax like expected from liquids. The above mentioned behavior results from the internal relaxation time spectrum of the materials which is right on the time scale of milliseconds to hours and as such similar to our daily experience. Materials with such characteristics are called soft matter and have a wide range of use in technical and medical applications reaching from lubrication to drug delivery agents. If generalized most living matter falls into this category as well.

Considering the above, it is important to classify and understand the mechanical properties of these materials and investigating their stress-strain relations is topic of a field called rheology. However, for highly viscose or viscoelastic materials performing reliable rheology is very challenging for several reasons. Due to the high internal friction in the material the mechanical continuum may break and surface slip, shear bands or fluctuations could emerge. Such local discontinuities will then show up in macroscopic observables like the viscosity probed in rheology. Since the mechanical load is always introduced by the solid boundary the near surface region might be of special interest and discontinuities may take their origin there.

Neutrons are an excellent probe to address such interface questions, since they interact with the nucleus of materials and not the electrons, like .e.g. x-rays. Therefore many materials are transparent to neutron radiation, for example silicon or quartz, whereas the hydrogen isotope deuterium has a comparability large scattering cross section. This enables grazing incidence scattering studies from solid-liquid boundaries. If this liquid is then consequently put under mechanical load, insights on the boundary can be gained. In this context neutron reflectometry is a well-established tool for probing the scattering length density profile along the surface normal. By using techniques like

GISANS or off-specular scattering, it is in addition possible to gain insights on lateral structures along the interface on different length-scales. Another advantage is that neutrons do not disturb the measurement as other methods that need direct contact with the sample, like for example atomic force microscopy, which takes a high risk of influencing the result. However which measurements are performed, the quality of an experiment is ultimately defined by the instrumentation. In this context the experimental set-up and data treatment may turn out to be in many cases the limiting bottleneck. One limitation, in particular for neutrons, is flux, which makes neutrons expensive and limits the possibility of studying kinetic processes.

In this thesis methods to combine inter-facial scattering and rheology of liquids under load have been developed in order to probe dynamical changes on the millisecond time-scale. Oscillatory rheology under conditions similar to loading-releasing processes of complex liquids for machine parts was carried out and the surface structure was monitored. In addition, complementary software tools for designing and evaluating grazing incidence scattering experiments have been developed. The goal of this summary is to provide the framework and introduction for the methods that are published in the papers rather than to reproduce textbook knowledge. The work is distributed into two parts, one focusing on soft matter science, with the other part focusing on neutron scattering, especially neutron instrumentation.

2. Neutron scattering

> If people do not believe that mathematics is simple, it is only because they do not realize how complicated life is.
>
> Janos von Neumann

In this chapter the most relevant parts of the theory are presented to describe neutron scattering experiments. The basic theory is analogue to x-ray scattering, with the difference that neutrons scatter from the nuclei while x-ray from electron. For a detailed overview the author recommends 'Element of modern X-ray physics'[1] and for further reading in regard to the Distorted Born Wave Approximation 'Liquid Surfaces and Interfaces'[2]. For a deviation of the equations from point scatters we refer to the articles of Sears [3, 4].

In this work exclusively coherent and elastic scattering is considered.

2.1 Neutron scattering

2.1.1 Historical context

Neutrons together with protons form the fundamental building block of nuclear cores. They were discovered 1932 by Chadwick in the Rutherford Laboratories [5]. He used the emission from a Polonium source and indirectly detected them via paraffin wax. In 1938 it was discovered by Lise Meitner, who migrated from Austria to Sweden like the author, Otto Robert Frisch and Otto Hahn, that neutrons are the driving force for nuclear fission [6]. Ironically, just Otto Hahn was awarded the Nobel price in chemistry (sic). Later they have attracted great interest during the Manhattan project, the US's efforts to militarise nuclear reactions. In this framework neutrons were first studied as a probe.

In Oak Ridge, TN, where a significant part of this project was conducted, the first neutron scattering experiments were conducted by Enrico Fermi and Walter Zinn in 1945 [7], which was published through declassification and then incorporated into Physical Review.

2.1.2 Neutron production and detection

Besides the use of Radioisotopes Californium 252 or Americium 242m as portable neutron sources through spontaneous fission, there are generally two ways of producing high flux neutron beams. Nuclear fission is used to harvest a constant neutron flux, at a so called reactor source, with the only exception of the PEAK pulsed reactor in Gatchina, Russia. Alternatively a high energy proton beam produced by a particle accelerator impinges on a heavy metal target and generates a pulsed neutron beam. This process is called spallation. The only accelerator without a duty cycle is the SNCS in Switzerland. A third promising, possible future, option is the use of an ignition laser to trigger a fusion reaction of a deuterium-tritium encapsulate [8].

In order to control the properties of the neutrons, they are collected in a moderator, e.g. for cold neutrons a coupled hydrogen moderator at low temperatures T = 20K, where they scatter inelastically. After a sufficient time they get equilibrated and will finally have the same energy/temperature as hydrogen in the moderator. Since the scattering is a statistical process the energy of the neutrons will satisfy a Maxwell Boltzmann distribution. This defines the spectral distribution of the source with a mean energy of $E = \frac{3}{2}k_bT$, k_b is the Boltzmann constant.
The deBroglie wavelength of the neutron is defined as

$$\lambda = \frac{h}{\sqrt{2m_nE}} \tag{2.1}$$

and a relation between energy and velocity v is obtained

$$v = \sqrt{\frac{2E}{m_n}} = \sqrt{\frac{3k_BT}{m_n}} \tag{2.2}$$

For the example of 20K this leads to a mean wavelength of $\overline{\lambda} = 5.6$Å. Typically neutron moderators are categorized with respect to temperature into hot (~1000 K), thermal (300 K) and cold (20 K) sources.
After the scattering experiment the neutron needs to be detected. Currently, to detect a neutron the following nuclear reaction is most commonly used:

$$^3He + ^1n \rightarrow ^3H^- + ^1p^+ \tag{2.3}$$

2.1.3 The neutron as a probe

Neutrons have several unique properties that make them interesting as a probe for materials science:

- The wavelength is in the range of inter-atomic distances in solids and fluids, which enables structural studies.
- The energy is comparable to molecular excitations in solids and fluids, enabling to directly access phonons and diffusion.

- The absorption of neutron in many materials is small allowing bulk studies of e.g. mechanical components or in this work inter-facial studies.
- The spin is directly sensitive to the magnetic induction in a material and as an example anti-ferromagnetism was first directly proven by the use of neutrons.
- Neutrons are non destructive for most materials, which makes them ideal for the study of proteins and other living tissue.
- Neutrons interact with the core and therefore different isotopes and light materials can be studied.

In the table below the properties of a neutron are displayed.

m_n	$1.6749510^{-27}kg$
$E(meV)$	$\frac{81.81}{\lambda(\text{Å})^2}$
$v(m/s)$	$\frac{3956}{\lambda(\text{Å})}$
μ	$-9.64910^{-27}JT^{-1}$
τ	$886 \pm 20s$

As seen in the table neutrons have a limited life time and their velocity changes with their wavelength. This behaviour is called dispersion and can be used to distinguish between wavelength.

2.1.4 Basic scattering

After defining the wavevector k of a neutron via the de Broglie wavelength λ scattering can be described by the difference between the incident and scattered wavevector, k and k', respectively.

$$\underline{q} = \underline{k} - \underline{k}' \tag{2.4}$$

$\underline{q}$ is the vector of momentum transfer. Here two different cases can be distinguised. If the length of the wavevector of the neutrons is conserved $|\underline{k}| = |\underline{k}'|$, no energy is transferred and the process is called elastic scattering. Equation 2.4 can be rephrased in dependence of the angle under which the detector is places, the so called scattering angle φ.

$$q = \frac{4\pi}{\lambda} \sin\frac{\varphi}{2}, \tag{2.5}$$

This is called elastic scattering, whereas if energy transferred, i.e. $E \neq E'$ the term inelastic scattering has been coined.

Mathematically scattering processes can be described by the Schrödinger equation:

$$\widehat{H}\psi = \left(-\frac{\hbar^2}{2m_n}\nabla^2 + V\right)\psi = E\psi \tag{2.6}$$

Here ψ is the wave function describing the neutron and V the scattering potential and E describes the energy of the neutron nucleus system. $\widehat{H}$ is called the Hamilton operator.
The cores of nuclei are usually on the scale of femtometers (1 Å=100000 fm) and thus the wavelength λ of the neutron can be assumed as being far larger than the scatterer. Neutrons interact with matter via the strong nuclear force (nuclear scattering) and though with the core of the atoms. An exception is magnetic scattering where the neutron interacts with unpaired electrons. Fermi described the nucleus as a discrete object with a Dirac delta-function δ and consequently one parameter (b) is sufficient to define the strength of the interaction between a nucleus and the neutron.

$$V(\underline{r}) = \frac{2\pi\hbar^2}{m_n} b\delta(\underline{r}) \tag{2.7}$$

This potential is called the Fermi pseudo potential. Here the constant $b \in \mathbb{C}$ is defined as the bound, i.e. the nucleus is not moving, scattering length $b = b' + \imath b''$. The complex number describes the scattering and absorption properties. The Schrödinger equation can be solved by a superposition of plane and spherical waves.

$$\psi(\underline{r}) = \exp(\imath \underline{k} \cdot \underline{r}) + \frac{\exp(\imath \underline{k} r)}{\underline{r}} f(\underline{q}) \tag{2.8}$$

Neglecting multiple scattering, extinction and at sufficiently large distance from the sample the scattering amplitude $f(\underline{q})$ is defined as the Fourier transformation of the scattering potential

$$f(\underline{q}) = -\frac{m_n}{2\pi\hbar^2} FT(V) = -\frac{m_n}{2\pi\hbar^2} \int V(\underline{r}) \exp(-\imath \underline{q} \underline{r}) d\underline{r} = -b. \tag{2.9}$$

To obtain a relation between the scattering amplitude and the differential scattering cross section, i.e. neutrons measured in a solid angle in space Ω, as an observable property the integral over the full sphere (indicated by 4π) can be taken as outlined in equation 2.11. The scattering cross section can then be calculated from the expectation value of the scattering amplitude and the phase information is lost:

$$\frac{\partial \sigma}{\partial \Omega} = |f(\mathrm{q})|^2 \tag{2.10}$$

The total scattering cross section is:

$$\sigma = \int d\sigma = \int_{4\pi} |f(\mathrm{q})|^2 d\Omega = 4\pi |b|^2 \tag{2.11}$$

It is composed out of three components for neutrons:

$$\sigma_{total} = \sigma_{coh} + \sigma_{inc} + \sigma_{abs} \tag{2.12}$$

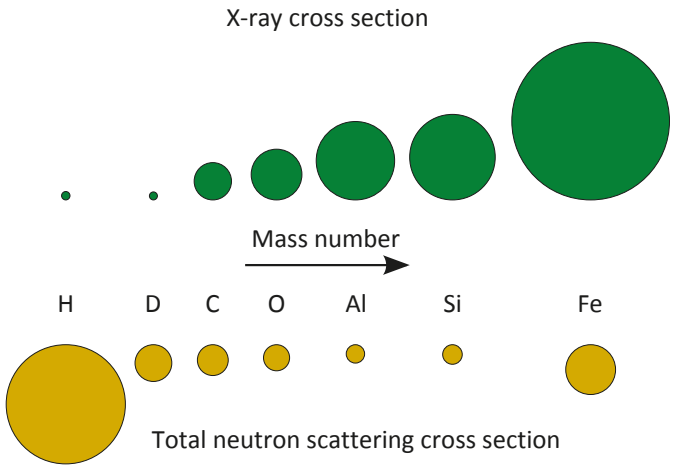

Figure 2.1. Reconstructed from NIST, National Ínstitut for Standards and Technology (NIST, Gaithersurg, MD). The total neutron scattering cross section σ_{total} is plotted for different elements. Interestingly silicon and aluminium have low cross sections, whereas hydrogen and deuterium exhibit totally different behaviour. It should be pointed out that hydrogen has a large incoherent scattering cross section while deuterium scatters mainly coherent. This gives rise to isotope contrasting.

Here σ_{coh} is the coherent , σ_{inc} the incoherent scattering cross section and σ_{abs} describes the absorption. Incoherent scattering is not preserving the phase and does not lead to interference. As a result it probes the particle self correlation function, which was not studied in this thesis and will thus be not considered any further. Still incoherent scattering goes to 4π and thus forms a constant background for coherent scattering studies. Considering this will merge the incoherent cross section into an effective absorption in this thesis. The scattering cross sections of some selected elements are summarise in figure 2.1.

2.1.5 Isotope contrasting

As aforementioned a main advantage of neutrons is that they interact with the core and not with the electrons in the shell. Therefore different isotopes have different properties to interact with neutrons. This gives rise to the field of isotope contrasting. The value of the scattering cross section is determined by aspects of nuclear physics and does not scale linearly with the mass number.

For instance the coherent scattering length for Hydrogen is -3.74 fm with a huge incoherent scattering length of 25.274 fm, whereas deuterium has a positive coherent scattering length of 6.67 fm and an incoherent scattering length of 4.04 fm.

This fact is extremely useful for the study of hydrogen containing materials and contrast variation, the exchange of hydrogen and deuterium is widely used in literature [9].

All properties of neutrons are collected by the US Department of Commerce, National Institute for standards and technology, NIST, Gaithersburg, ML [10] and are available for review electronically. In addition to contrast variation materials that are transparent (or almost transparent) for neutron radiation can be used to study samples in complex sample environments with minimum disturbance. As an example the following materials have a high transmittance for neutrons and can depending on the specific applications be employed as sample containers for neutron scattering studies:.

- aluminium (5080P to avoid gamma activation and or magnetization)
- low doped silicon
- quartz glass or sapphire for light transparency
- specially composited alloys, so called null matrix alloys, can show neutron transparency in combination to excellent mechanical, chemical and thermal quality [11].

2.2 Reflectometry

> "What shall we look for, and what shall we see?"
> "What you will see, if you leave the Mirror free to work, even the wisest cannot tell."
>
> Frodo Baggins and Lady Galadriel about surface scattering

Neutron reflectometry and small angle scattering (SANS) describe experiments at small momentum transfers. As a result large length scales are probed and the details on an atomic length scales are not resolved. Therefore instead of using discrete scattering potentials assigned to individual atoms a more macroscopic approach is used and the so called scattering length density is introduced as scattering potential. The principles of scattering at small momentum transfers are outlined in this chapter.

2.2.1 Basic reflection

Usually, for reflectometry studies the coordinate system is defined with respect to the sample surface. The geometry is displayed in figure 2.2.

Specular reflectivity is defined for an equal incident and exiting beam angle with respect to the interface $\alpha_i = \alpha_f$. The momentum transfer is then perpendicular to the surface along the surface normal. Neutron reflectivity can be described similar to optics by introducing a refractive index n and using of Snellius law

$$n_1 \sin \alpha_i = n_2 \sin \alpha_i' \tag{2.13}$$

with α_i and α_i' the beam angles with respect to the interface above and below. Mathematically, reflection studies can again be described by a Schrödinger equation:

$$\nabla^2 \psi(\underline{r}) + k^2 \psi(\underline{r}) = 0 \tag{2.14}$$

However, since the interface is plane in this case no spherical waves are needed and the superposition of plane waves is sufficient but with a changed momentum inside the material:

$$k^2 = \frac{2m}{\hbar^2}(E - < V(\vec{r}) >) \tag{2.15}$$

The refractive index can then be defined as the ration between the wave vectors above and below the interface:

$$n^2 = \frac{k^2}{k_0^2} = 1 - \frac{V_0}{E} \tag{2.16}$$

And the scattering potential is now the averaged potential:

$$V_0 = \frac{2\pi\hbar^2}{m} SLD \tag{2.17}$$

The average density of the Fermi pseudo potential directly leads to the definition of the optical properties and the refractive index n. The scattering length density SLD is the number density of scatterers multiplied with their respective scattering length and can be defined as the sum of all scattering lengths b per volume element V. This property inherently includes the chemical density of the material.

$$SLD = \frac{\sum_i b_i}{V} \tag{2.18}$$

This leads to following definitions of the refractive index.

$$n = 1 - \lambda^2 A + \imath\lambda B. \tag{2.19}$$

$$\begin{aligned} A &= \frac{\Delta b_{\text{coh}}}{2\pi} \\ B &= \frac{b_{\text{abs}} + b_{\text{inc}}}{4\pi} \end{aligned} \tag{2.20}$$

Again, here Δb represents the bound coherent scattering length and $\sigma_{\text{abs}}, \sigma_{\text{inc}}$ represent the absorption and incoherent cross section respectively. From Snell's law it is clear that for certain incident angles the incoming wave might not penetrate the surface it impinges and total external reflection may occur. The critical angle of total external reflection is defined as:

$$\sin\alpha_c = \lambda_i \sqrt{\frac{SLD}{\pi}} \tag{2.21}$$

Analogue for a given incident angle a critical wavelength can be defined:

$$\lambda_c = \frac{\sqrt{\frac{SLD}{\pi}}}{\sin\alpha_i} \tag{2.22}$$

To vary the momentum transfer apparently the impinging wavelength α_i or the impinging wavelength λ_i can be varied. This describes the two modes to operate reflectometers, angle dispersive measuring or wavelength dispersive, respectively. For specular reflectivity the momentum transfer perpendicular to the surface can be written as

$$q_z = \frac{4\pi}{\lambda}\sin\alpha_i = \frac{4\pi}{\lambda}\sin\alpha_f \tag{2.23}$$

What is fundamental for all experiments is that the importance of instrumentation can not be underestimated.

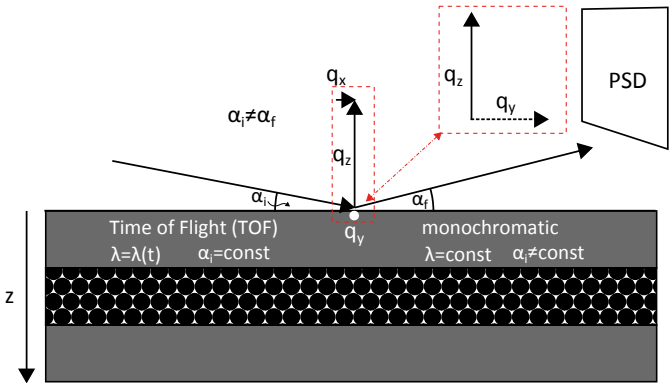

Figure 2.2. Commonly used geometry in all surface near scattering experiments. The two different ways to run a reflectometer are outlined, as well as how the position sensitive detector (PSD) is placed in regard to the coordinate system and the sample surface.

2.2.2 Bragg law in layers

For a layered system, as shown in figure 2.3, the Bragg condition can be derived geometrically. Constructive interference, meaning the wave reflected at the two interfaces (the red and blue line) have the same phase at the same time, occurs if the path difference is equal to a multiple of the wavelength λ.

$$|\underline{AB}| + |\underline{BC}| - |\underline{AC'}| = n\lambda \tag{2.24}$$

Over trigonometric functions this leads to the Bragg equation:

$$n\lambda = 2d\sin(\alpha) \tag{2.25}$$

For layered systems this gets naturally more demanding if the optical properties in the different layers change. This can be extended to a modified Bragg law for multi-layers [12].

2.2.3 Kinematic description

Similar to the calculation of the scattering amplitude described above the envelope of the reflected intensity can be described in Born approximation as well. Note: The result has still to be weighted with the Fresnel reflectivity, but roughness and inter-diffusion can then be assessed by the Fourier transform of the changes in scattering length density:

$$Rq_z \doteq R_f(qz)\left(\frac{1}{SLD_\infty(z)}\int \frac{\partial SLD(z)}{\partial z} e^{iq_z z} dz\right)^2 \tag{2.26}$$

The master formula can be seen as a coherent sum over the scattering amplitude perpendicular to the sample. From the equation it is clear that the specular

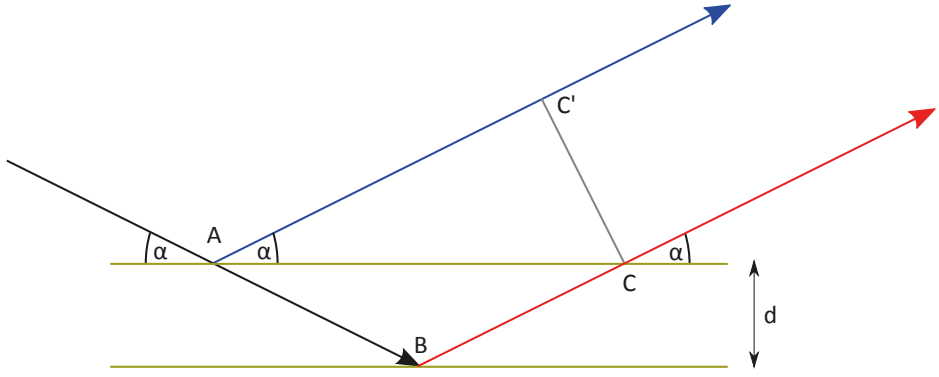

Figure 2.3. A geometric derivation for Bragg's law. The path length between the red and the blue line needs to be a multiple of the wavelength λ in order to see constructive interference.

reflectivity is sensitive to changes in scattering length density perpendicular to the surface. In kinematic approximation this suffices to cover for one dimensional roughness as illustrated in figure 2.4 and will be outlined in chapter 2.2.5.
Since there is no easy way to access the phase information, there are many different profiles possible resulting in having the same reflectivity. This is known as the phase problem and its possible ramifications are illustrated in figure 2.5. Interestingly by using ferro-magnetically tunable top layers, it would in theory be possible to solve the phase problem for reflectometry [13, 14].
However for Born Approximation dynamical surface effects like critical reflection is not taken into account.

2.2.4 Dynamic description

The considerations in the last paragraphs did not take into account that the waves get actually refracted at the interface. However, this problem can be solved in perfect analogy to optics. Below the critical angle α_c, or the corresponding critical wavelength λ_c, total reflection occurs. For a single interface above a certain value the scattering can be described with the so called Fresnel

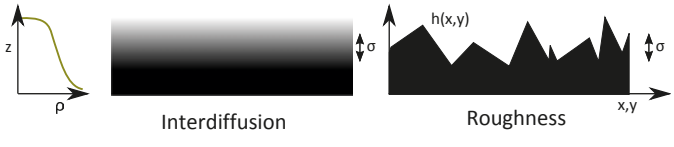

Figure 2.4. The averaging specular neutron reflectivity can not distinguish between inter-diffusion and geometrical roughness, left and right panel, respectively.

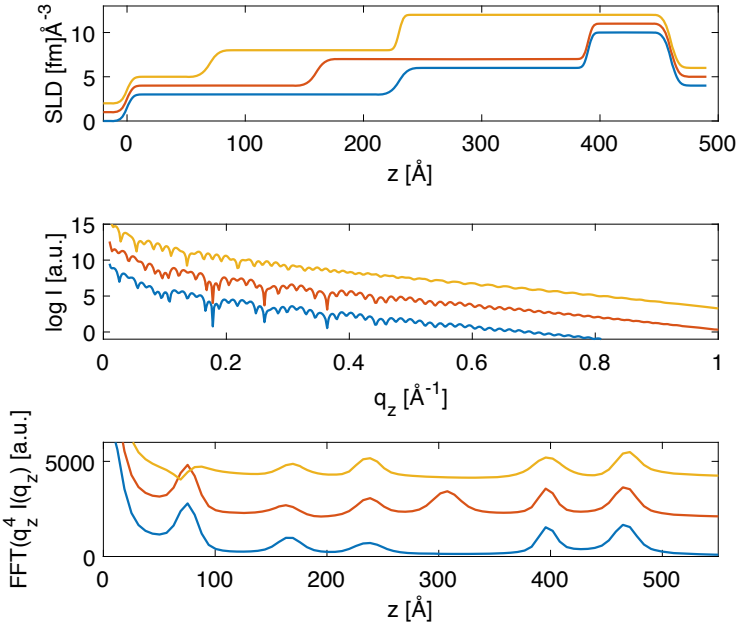

Figure 2.5. Illustrating the phase problem. For illustration purposes an offset was introduced in all the panels. In the top panel three different SLD profiles are shown. The layer thickness were 70/160/230 Å 160/230/70 Å and 230/160/70 Å respectively. Panel 2 shows the reflectivity emerging from the SLD profiles. The red and blue graphs are almost identical. The bottom panel shows a frequency analysis. Surprisingly the distances of the yellow and blue curves are identical, whereas there is one distance (320 Å) that contributes to the scattering picture. The reflectivity for the green and red picture is almost identical, whereas the yellow curve deviates strongly. These three cases illustrate that a direct reconstruction out of the scattering signal is impossible without knowledge of the phase. (The idea is a courtesy of Dr. Seeck from DESY, Hamburg, Germany)

equation 2.27

$$R_f(q_z) = \frac{k_c^4}{q_z^4} \tag{2.27}$$

At every interface the wave amplitude and it's derivative have to be continuous. This fact can be used to derive a general recursion formula as given in the paper by Parrat in 1954 [15]. The wave-vector transfer combined with the dampening leads to a ratio X between reflected R and transmitted T wave at every layer surface.

$$k_z, j^2 = (n_j k)^2 - k_x^2 = (1 - \lambda^2 A + \imath\lambda B)^2 k^2 - k_x^2 \tag{2.28}$$

$$r_j = \frac{k_z, j - k_{z,j+1}}{k_z, j + k_{z,j+1}} \tag{2.29}$$

$$X_j = \frac{R_j}{T_j} = e^{-2\imath k_{z,j} z_j} \frac{r_j + X_{j+1} e^{2\imath k_{z,j+1} z_j}}{1 + r_j X_{j+1} e^{2\imath k_{z,j+1} z_j}} \tag{2.30}$$

These equations incorporate the Lambert Beer law for extinction. By using the continuation condition of each interface, it is possible to recursively calculate the scattering by using the formulas of Parrat, which is illustrated in figure 2.6.

Alternatively a method called matrix method [16] can put the recursion together:

$$B_j = k_{z,j} \cdot z_j \tag{2.31}$$

$$u_j = \begin{bmatrix} e^{B_j} & r_j e^{B_j} \\ r_n e^{-B_j} & e^{-B_j} \end{bmatrix} \tag{2.32}$$

$$M = \prod_j u_j, \tag{2.33}$$

$$R = \left|\frac{M_{11}}{M_{21}}\right|^2 \tag{2.34}$$

This leads to a tool to analyse layered structures in thin film science. For a complete deviation of the matrix formalism, used in computer programs, we refer to the literature [1, 17, 18] or descriptions of available software (e.g. GenX [19]).

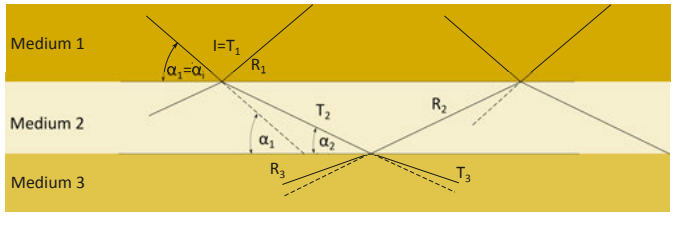

Figure 2.6. Reconstructed from [15]. Illustrates how the recursive algorithm can be derived geometrically.

Figure 2.7. The picture of Södermalm (pixabay creative commons) illustrates a rough mirror. Specular scattering, i.e. the mirror image, and incoherent effects, the blur can easily be spotted.

2.2.5 Roughness

In figure 2.7 the difference between coherent and diffuse scattering contribution is illustrated and can easily be seen at the imperfect mirror image from an ice surface. In the context of reflectometry roughness is usually treated as a smearing on the SLD profile as described in section 2.2.3.

In general there are two effects which can blur the SLD at an interface as illustrated in figure 2.4 and for the depth profile chemical (inter-diffusion) roughness is treated the same way as physical (geometric) roughness.

In the important paper of Sunil Sinha [20] a concise concept of surface roughness with fractal self affinity was introduced, that can describe surfaces roughness as Gaussian distributed, leading to the error function in equation 2.35. The roughness, as parameter of the error function, can be propagated in the Parrat algorithm by the use of the Nevot Croce factor [21] equation 2.36 that leads to the Debeye Waller factor [22] equation 2.37 if the roughness is assumed to be symmetric in both direction. The error function leads to the Debeye Waller factor directly from the master formula via Fourier transformation, and Q_j resides for a smooth interface as unity.

$$erf(z) = \frac{1}{\sqrt{2\pi}\sigma} \int_0^z e^{-\frac{-u^2}{2\sigma^2}} du \tag{2.35}$$

$$Q_j = e^{-2\sigma_j^2 k_j k_{j+1}} \tag{2.36}$$

$$Q_j = e^{-2\sigma_j^2 k_j^2} \tag{2.37}$$

Here σ describes the roughness as standard deviation of a Gaussian distribution as outlined in figure 2.4.

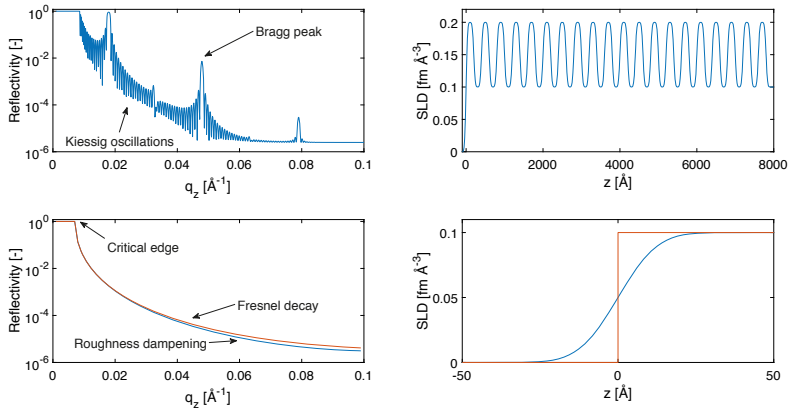

Figure 2.8. In the inlays the SLD profile and the emerging reflectivity curves are depicted to provide an overview on how different reflections may emerge out of SLD profiles. The case of a periodic layered structure and a single interface are depicted, upper and lower panels, respectivley.

By including in the Parrat algorithm in equation 2.29 a full description of one dimensional roughness can be given.

$$r_{j,rough} = r_{j,ideal} \cdot Q_j \tag{2.38}$$

Alternatively, if the roughness of an adjacent layers is larger than the layer itself, slicing, the use of very small slabs with a gradient in SLD can be used to avoid unphysical bias. Reflectivity curves for different SLD profiles are plotted in figure 2.8.

2.2.6 Penetration depth

In the same paper of Parrat [15] the mean penetration depth $d_{\frac{1}{e}}$ of a neutron wave into a material is depicted as a function of the incident angle, the incident wavelength and the coherent and incoherent scattering cross section.

$$d_{\frac{1}{e}} = \frac{\frac{\lambda_i\sqrt{2}}{4\pi}}{\sqrt{\sqrt{(\alpha_i^2 - \arccos(1 - A\lambda_i^2)^2)^2 + 4B^2\lambda_i^2} - (\alpha_i^2 - \arccos(1 - A\lambda_i^2)^2)}}. \tag{2.39}$$

The value corresponds to the complex refractive index n as outlined in equation 2.19. In figure 2.9 the penetration depth is displayed for one specific example (A and B for values of 1.43 10^{-6}Å^{-2} and 2.96 10^{-9}Å^{-1}) and plotted over the incident wavelength λ_i and the incident angle α_i. Notice the steep step at

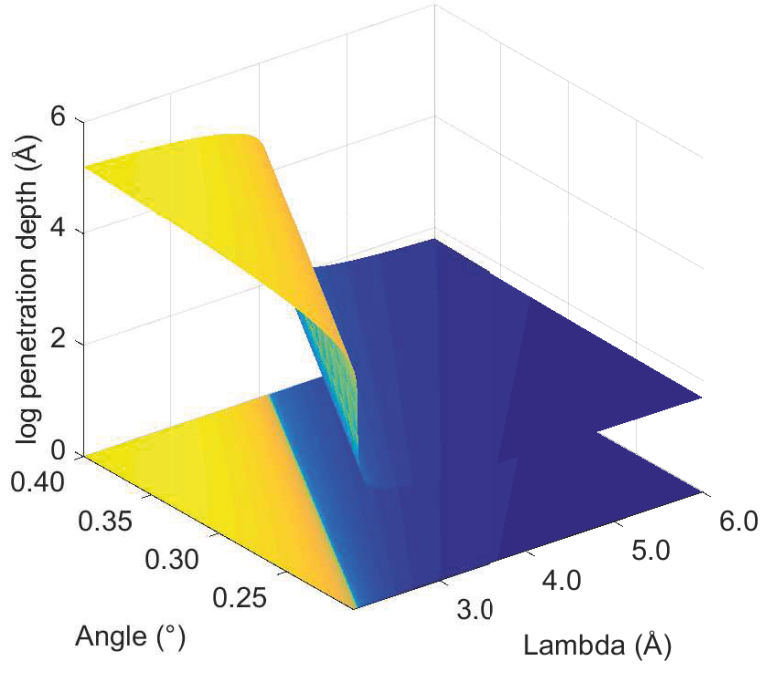

Figure 2.9. An example of the penetration depth $d_{\frac{1}{e}}$ (equation 2.39) plotted over the pair of incident wavelength λ_i and the incident angle α_i. A and B was kept at 1.43 10^{-6}Å^{-2} and 2.96 10^{-9}Å^{-1}, respectively.

the critical edge, which essentially separates into three different regimes. The surface region, the bulk region and the intermediate edge region. The characteristic lines (here lines between two colour areas) are not parallel, which is an indication that an easy convolution of the two variables is not always possible. Combining those with the Fresnel equations and the Lambert Beer law of extinction leads to a description of the penetrating flux I normalized by the incident flux I_0 into a reflectivity sample as outlined in paper VI.

$$\frac{I}{I_0} = T_{\text{Fresnel}}(\lambda, \vartheta_i, A, B) e^{-\frac{z}{d_{\frac{1}{e}}}} \tag{2.40}$$

2.2.7 Resolution effects

As described in the last section, for low absorbing probes, like neutrons, the penetration depth increases steeply at the critical angle of total external reflection. This imposes severe challenges with respect to instrumental resolution if one would like to study surface structures with depth sensitivity. The small

incident beam angles make this considerations even more severe. Note in this context that for infinite resolution the flux would be zero. To simulate reflectivity the values for angular divergence and incident wavelength spread are usually assumed to be very sharp and folded with a Gaussian to account for deviation. This should be seen in relation to photon sources where the brilliance is 10 orders of magnitude (even five for lab machines) higher than for a neutron source. Thenceforth the resolution of neutron beams can not be narrowed down too much.

Generally resolution is treated with fast convolution of a Gaussian bell function and Gaussian error propagation [23]. Commonly the resolution function is called resolution ellipsoid technically describing three axis machines. A typically used double slit will produce a trapezoid or if specifically set a triangular function. Fermi Choppers will result in a trapezoid function as well. A typical velocity selector gives a triangular PDF (probability density functions). It is important to note that this is desirable, since all the just mentioned distributions drop to zero beyond a certain cut off in wavelength and angle implying that other than for Gaussians no contributions for incident beam angles and wavelength far from the desired ones have to be taken into account. In paper VI an explicit smearing kernel, as described for specular reflectivity by Andrew Nelson [24], had been developed to take into account resolution effects for all grazing incidence neutron scattering experiments. There is strong evidence that the convolution of the angular and the energy distribution can potentially produce misleading results and a full treatment with two dimensional PDF is necessary. By taking the penetration depth described above as visualized in figure 2.9, it is similar to taking cupcakes over this distribution and then adding together the normalized scattering data. If the resolution function is sufficiently wide a broad range of different penetration depths is probed. For time of flight experiments a convolution with the moderators spectral emission density and their uncertainty has to be done in addition:

$$I(\lambda) = \tilde{I} \otimes MES(\lambda) \tag{2.41}$$

2.2.8 Off specular scattering and GISANS

In the aforementioned theory, just the intensity of the specular reflection was calculated. As visible in figure 2.4 roughness can have lateral correlations should be described with the roughness profile $h = h(x,y)$.

In Born approximation the non specular scattering amplitude can be derived similar to equation 2.9. Now the scattering is not resulting from atoms but roughness.

$$f(\underline{q}) = \int_V \triangle SLD \cdot \Theta(z - h(x,y)) e^{\imath \underline{qr}} dV \tag{2.42}$$

Θ here depicts the Heaviside-theta function, that is 0 for negative arguments and 1 for positive numbers (including 0).
The roughness leads to diffuse scattering in all directions. If the height variation of $h(x,y)$ are correlated in x and y direction a resonant signal emerges and can be described again with the Bragg equation 2.3.

Examples for that could be correlated roughness or an ordered surface structure. By accessing different regions of q_x and q_z, information of lateral structures in the plane can be obtained. The off-specular scattering can be seen in figure 2.10. The lines normal to the specular ridge are called Bragg sheets and occur from correlated roughness if the roughness. Off-specular scattering is defined as scattering, where the incident and exit angle of the beam are not equal, i.e. $\alpha_i \neq \alpha_f$, as for specular reflection, but still in the same plane (see figure 2.2). Scattering out of the scattering plane is called grazing incidence small angle scattering GISAS and provides the possibility to study in plane correlation on surfaces on smaller length scales. For typical incident beam angles of, e.g. 0.3, in grazing incidence geometry length-scales of around 100 micometer are probed in off-specular scattering along the x direction, which is in contrast to the smaller (up to 1 micrometer) length-scale probed in z direction. GISAS was first invented was invented in 1989 for x-rays [25] and was then used first with neutrons in 1994 by Bill Hamilton [26]. A main difference to SANS is that the effectively probed volume and therefore the signal strength is a function of the incident angle and wavelength [27].

By varying the incident angle α_i and the incident wavelength λ_i and use of equation 2.39 the mean depth of where the signal emerges can be tuned. Ay a solid-liquid boundary Lambert Beer's law can be used to weight the signal and describe from which depth the lateral scattering emerges. Paper VI describes the process of statistical weighting. It is shown, that accessing the information of a buried layer will under no condition dominate the signal, but can be extracted via reverse transformation.

If angles typically used, e.g. 0.3°, in grazing incidence geometry are put into equations 2.43, length-scales of around 100 μm are probed for the x direction of the momentum transfer, which is in contrast to the maximum of 1 μm length-scale probed in z direction.

Paper I describes an example of penetration depth variation for GISANS on a time of flight reflectometer. An overview of the technique is given by Alexander Hexemer [28]. Theoretically the non-specular scattering can be described by the distorted wave born approximation DWBA. In short this is a first order perturbation theory, where the signal emitted from a certain depth is calculated in Born approximation but the intensity is weighted with the wave amplitude at this specific depth. For a more thorough description we refer to Boris Toperverg [29], Jan Burle [30] and Remi Lazzari [31].

2.2.9 Data representation

Generally, to compare diffraction data to theory or simulations it is necessary to have the scattering function represented in q space. For reflectometry geometry the transformation of the coordinates is as follows:

$$\begin{aligned} q_z &= \frac{2\pi}{\lambda} \cdot (\sin\alpha_i + \sin\alpha_f) \\ q_y &= \frac{4\pi}{\lambda} \cdot \sin\psi \\ q_x &= \frac{2\pi}{\lambda} \cdot (-\cos\alpha_i + \cos\alpha_f) \cdot \cos\psi \end{aligned} \tag{2.43}$$

These are defined out of figure 2.2. Ψ depicts the angle between projected to XY plane between the scattered and the reflected beam. The equations in 2.43 show a highly non linear way of displaying data. Since the detectors are typically not spherical it is challenging to transfer data without artefacts.
For monochromatic instrument usually the intensity is plotted for sets of incident and exitent angles α_i, α_f, whereas for time of flight machines so called RTOF data, a map of detector angle α_f over incident wavelength λ_i, is displayed.
There a two ways to visualize reflectivity data outside of instrument detector space:
a) Plotting the incident wave vector p_i over the exiting wave vector p_f
or
b) transferring everything to momentum transfer space [32, 33, 34].

The different possible illustrations are depicted in figure 2.10. The second option allows a direct comparison to physical models but has the disadvantage that the data becomes strongly compressed close to the critical edge. Paper IV describes a method to convert data between the above mentioned possibilities. The particular challenge that is addressed is the re-binning of the data to rectangular grids to overcome the strong non-linearity of the transformation and to access directional cuts.

2.2.10 Data correction and normalisation

To extract a meaningful physical representation from counted neutrons it is not enough to transfer the data into momentum transfer space. Additionally a normalisation to the incident beam and a background signal reduction is needed [34, 35, 36].

$$I_{abs} = \frac{I}{I_0} = \frac{\frac{I_{meas}}{pc_{meas}}}{\frac{I_{directbeam}}{pc_{directbeam}}} \tag{2.44}$$

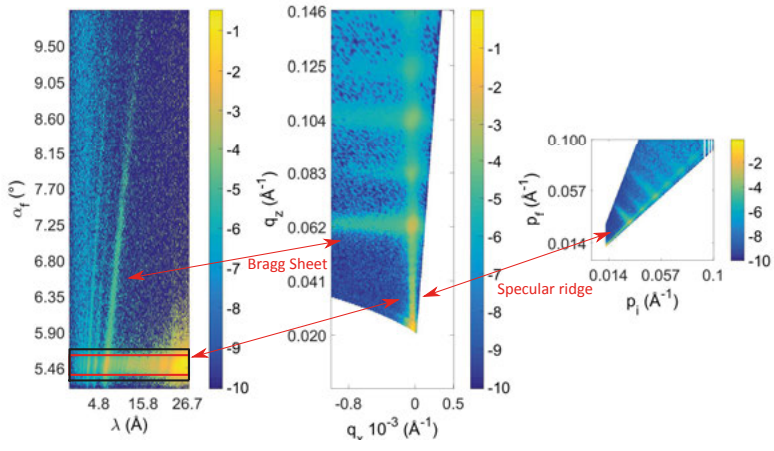

Figure 2.10. Three different common ways to display reflectivity data. Left in instrument space, in momentum transfer space in the middle and *pi* vs pf (momentum space) in the right panel. Clearly visible is the specular reflectivity within the red box and the region often used to subtract the background for specular experiments in the black box.

Here pc is the normalization value defined as the accumulated measuring time weighted by the neutron production power during the measurement.

$$pc = \int P(t)dt \tag{2.45}$$

There are different ways to determine pc. Either by the usage of monitors or by using the reactor power over time for reactor sources or the proton charge on target for spallation sources, respectively. If the direct beam can not be measured directly alternatively software can be used to calculate this value from an attenuated measurement.
The value I (in counts) is subject due to the discretization of detector bins and can be derived by :

$$I = \sum I_{bins} - \overline{I_{bkg}} \tag{2.46}$$

The exact region of the specular reflectivity is difficult to determine as there is always smearing and diffuse scattering superimposes.

The whole reduction process relies on weighting average and error propagation. In this context it is necessary to define a ROI (region of interest), i.e. marking the specular reflection and the background as outlined in the left panel of figure 2.10.

In paper IV, the problem is further discussed and the appendix 8.3 provides a possible way for accurately normalising specular reflectivity data.

2.3 Additionally used techniques

> A drunk man will find his way home, but a drunk bird may get lost forever.
>
> George Pólya

2.3.1 SANS

Small Angle Neutron Scattering (SANS) is a good way to investigate soft matter. It is possible to simultaneously probe the particle shape and composition (for example core shell, radius of gyration), the particle interaction and possible cluster formation. The form factor represents information for the shape of the scatterer whereas the structure factor provides information about the interaction between the particles. The SAS intensity can be expressed as a function of the scattering vector q, i.e. the wave-vector transfer between the incoming and the scattered radiation, as a complex integral over the volume for sufficient averaging.

$$I^{SAS}(\underline{q}) = |\int_V SLD e^{\imath \underline{q}\cdot\underline{r}} dV|^2 \tag{2.47}$$

Again this is in Born Approximation, therefore this Fourier transform of the form factor can be seen as an analogy to the master's theorem (equation 2.26) and the initial definition of Born approximation (equation 2.9) neglecting the structure factor.
The typical geometry is outlined in figure 2.11. It is obvious that the position sensitive detector provides several values of q together with a corresponding intensity in a single shot by measuring different scattering angles. A challenge in this context is to do an azimuthal integration. (For a further discussion, we reference to the NIST software). For a more thorough description, we refer to the literature of Oskar Glatter, Jan Skov Pedersen and Peter Fratzl [37, 38].

2.3.2 Stroboscopic technique to overcome flux limitations

The study of kinetic processes becomes more and more important in science. A lot of these processes can be studied well with photons in so called pump probe experiments, where the sample is exited and then the response is observed.

With neutrons this is only possible, if the changes are sufficiently slow. However most mechanical processes are so fast, that the flux of neutrons is not sufficient.

If repeatable processes are observed adding up several scattering signals the flux can be accumulated, which was first described by Robert Dalgliesh in 2004 [39]. These so called stroboscopic experiments become apparent if the brightness of a neutron beam is compared to a light bulb and are 20 orders of magnitude beneath modern undulators or even free electron lasers (FEL).

We developed a technique that took advantage of measuring every neutron as a single event, so called event mode data collecting. These events all can be traced with GPS time stamps. By using an apt sampling frequency data on the exciting property, e.g. mechanical stress or magnetic fields, can be included into the event stream. The neutron events can then be reassigned to additional information and scattering pictures for each stage of the transition can be extracted.

In figure 2.12 the main idea of the method is described. Events get reassigned to certain stages in an exciting wave form. This becomes more relevant in terms of data mining as often used in other disciplines, for instance astronomy, since all kinds of supplementary data can be included in the event stream.

The technical aspects and implications are described in detail in paper II and the dual frequency modulation that arises from using time of flight machines is discussed in paper VII. An example of data is presented in a later section figure 3.7.

This method is in contrast to TISANE [40][41], where the spectral contributions are split out and integrated spatially. This requires perfect synchronicity of the excitation to the neutron beam frequency.

A curious thing is that a similar process is described for undulators [42]. This means that this challenge is not unique to neutron scattering experiments.

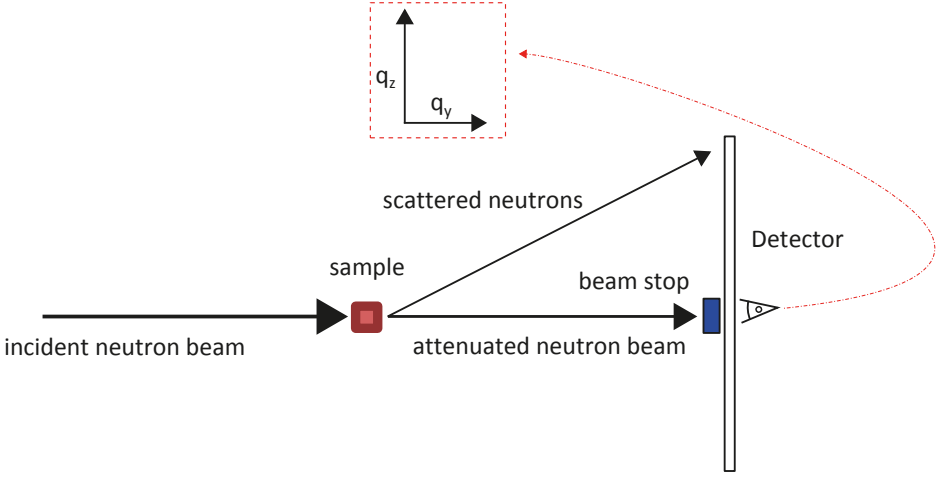

Figure 2.11. Typical small angle geometry.

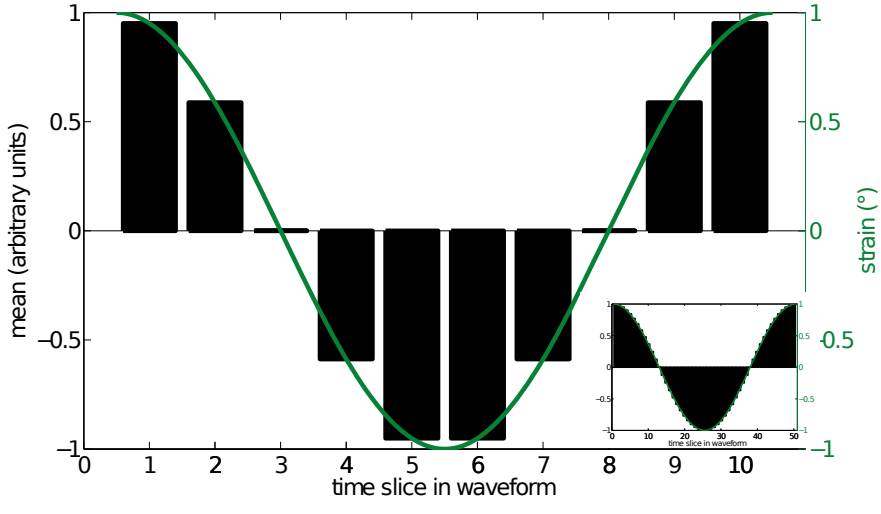

Figure 2.12. The picture illustrates how the distribution on the waveform works and how the reintegration works. Reprinted with the kind permission of the publisher(IUCR).

3. Soft matter

> With four parameters I can fit an elephant, and with five I can make him wiggle his trunk.
>
> Janos von Neumann

In this chapter an overview of the basic concept of soft matter science, rheology and surface slip effects is given. Since this field has reached an enormous size, it is referenced to the literature for further reading.

In general soft matter can be described as having properties both being liquid and solid on time-scales of human observation, i.e. milliseconds to seconds. DeGennes, the father of soft matter, got the Nobel prize in physics 1991 for his contribution to discovering that methods developed for studying order phenomena in simple systems can be generalized to more complex forms of matter, particularly to liquid crystals and polymers [43, 44].
Many important aspects like self-assembly especially in bio- and polymer physics are typical soft matter fields and a lot of emerging properties from the micro-structure can be observed. Examples here would be liquid crystals (LCDs), sol gel transitions and most importantly, all living matter.

3.1 Rheology

In the field of rheology the stress strain relation in matter is studied and the main quantity addressed is the viscosity η. The general equation 3.1 describes the stress τ as a function of shear rate $\dot{\gamma}$. The viscosity can be seen as the resistance to shear deformation of the material as is outlined in figure 3.1.

$$\tau = \eta \cdot \dot{\gamma} \tag{3.1}$$

In fact the viscosity can be generalized as a tensorial equation for anisotropic media and η becomes a hyper tensor.

$$\underline{\underline{\tau}} = \underline{\underline{\underline{\eta}}} \cdot \underline{\underline{\dot{\gamma}}} \tag{3.2}$$

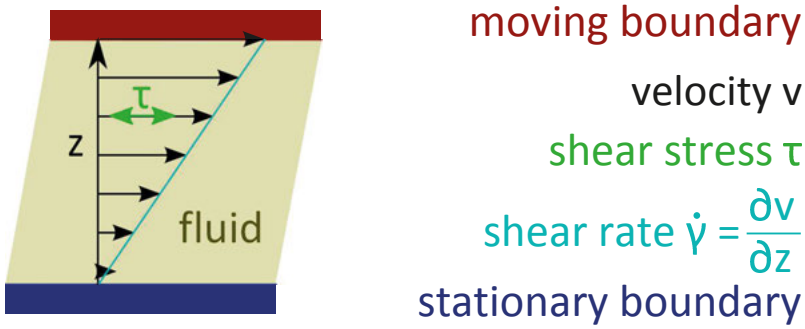

Figure 3.1. The geometric definition of the viscosity is displayed and gives a visualization of the used properties between two sheared plates.

3.2 Flow behaviour

The main constitutive equation 3.1 can be complicated $\eta = \eta(\dot{\gamma}, t)$ with being a function of strain rate and time. By assuming an isotropic behaviour and focusing on one dimensional cuts, it is possible to distinguish different examples. These can be illustrated by plotting the shear stress over shear rate in figure 3.2. Note that the viscosity η is the gradient of the flow curves.

3.2.1 Rate dependent behaviour

All the following examples refer to figure 3.2 and provide an overview. A more complete overview with examples can be found in the book of G.K. Batchelor [46].
Newtonian fluids describe a group of fluids where the stresses caused by their flow are linearly proportional to the applied shear rate. Examples for Newtonian fluids would be water or alcohol. If there is a threshold, the behaviour called Bingham dilatant is outlined and typical examples for that would be tooth brush or chocolate. Shear thinning (curve three) is observed if the viscosity decreases with increasing shear rate, like the dangerous quicksand or most noteworthy blood. Other than the examples just mentioned also most polymers are shear thinning. This relates to their relaxation spectrum or structural re-arrangements under shear. Casson plastic fluids (type one) can be observed if after a threshold shear thinning takes place. Here, molten ice cream or ketchup could be named. Dilatant or shear thickening fluids increase in viscosity if under load, as silica in Polyehtylene gycol.

3.2.2 Time dependent behaviour

If the rheological properties change with time of loading, two different properties can be observed. With thixotropic fluids the viscosity decreases over time.

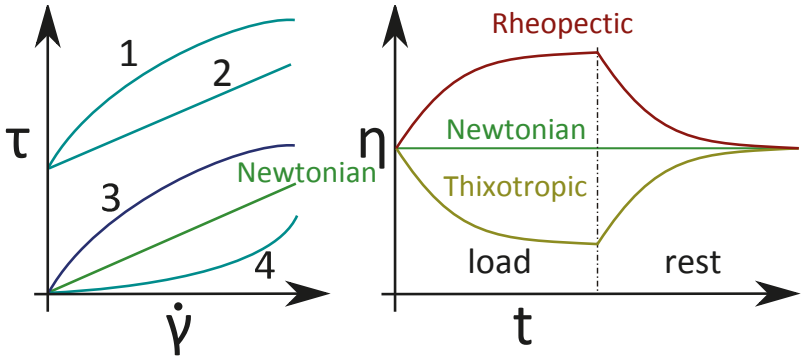

Figure 3.2. On the left hand side possible shear rate dependencies of viscosity are displayed. The green line depicts Newtonian behaviour. Curve 1 depicts casson plastic, 2 bingham dilatant, 3 shear thinning and 4 shear thickening. On the right hand side time dependent viscosities are shown. The red and wood coloured lines are thixotropic and rheopectic regimes, respectively. Again the green line corresponds to Newtonian behaviour.

Thixotropy is the base state of all bodily fluids (with an exception of synovial fluid) and colloidal suspensions [45]. Rheopectic (often called inverse thixotropy) is an increase of viscosity with time, e.g. gypsum paste and the named synovial fluid. This is different from so-called memory effects, where the properties are changed due to a phase transition.

3.3 Visco-elastic materials

Soft matter typically shows mechanical properties of a liquid and mechanical properties of a solid. This behaviour is called visco-elasticity since both a Young's modulus E (as stiffness) and a viscosity η can be assigned to describe the behaviour. A dash-pot is a mechanical device, a damper which resists motion via viscous friction over time t and a spring is a device that stores energy proportionally to the elongation ε. A combination of one spring and one dash-pot is used as the so called Maxwell model to model the stress σ and strain ε relation as described in the constitutive equation 3.3:

$$\frac{1}{E}\frac{\partial\sigma}{\partial t}+\frac{\sigma}{\eta}=\frac{\partial\varepsilon}{\partial t} \tag{3.3}$$

If many of those elements as displayed in figure 3.3 are connected with different sets of viscosity η and Young's modulus E different relaxation modes can be modelled. This is called generalized Maxwell model, which is also known

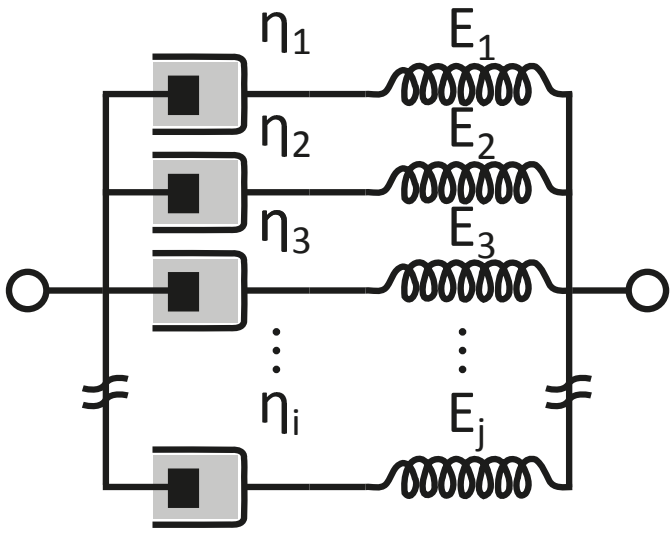

Figure 3.3. Picture of a generalize Maxwell-Wiechert element. A dash-pot that is combined with a spring to account for viscous and elastic behaviour is called a Maxwell element. The illustration shows a coupling of a set of Maxwell elements, typically used to describe visco-elastic materials. The different sets of springs and dash-pots account for different relaxation times.

as the Maxwell–Wiechert model. Essentially this can be seen as a dampened harmonic oscillator with different time constants.

3.4 Oscillatory rheology

By applying a cyclical load in form of a sinusoid waveform, a versatile tool to investigate soft matter is available.

By defining the strain as a sinusoid waveform and measuring the mechanical stress, following equations can be derived in analogy to an excited harmonic oscillator with dampening. This can be done as long as the model for the complex fluid is a generalized Maxwell spring, which is the general form to describe visco-elasticity.

$$\begin{aligned} \varepsilon &= \varepsilon_0 \sin \omega t \\ \sigma &= \sigma_0 \sin \omega t + \delta \end{aligned} \tag{3.4}$$

Here, the excitation ε is a sinus function where $\omega = 2\pi f$ is the angular frequency over time t. The measured stress σ, the response function, is then

assumed to have the same shape with a phase shift δ.

$$\begin{aligned} G^*(\omega) &= G'(\omega) + iG''(\omega) \\ G' &= \frac{\sigma_0}{\varepsilon_0}\cos\delta \\ G'' &= \frac{\sigma_0}{\varepsilon_0}\sin\delta \\ \sigma(t) &= G'(\omega)\gamma_0 \sin\omega t + G''(\omega)\gamma_0\cos\omega t \\ \tan\delta &= \frac{G''}{G'} \end{aligned} \tag{3.5}$$

This consequently introduces the complex modulus out of G' the storage and G'' the loss modulus, respectively. The tangent of these two moduli, $\tan\delta$, is the mechanical dampening factor and is a measure for loss. This opens the door to the field of oscillatory rheology [47, 48], where the response of the sinusoid excitation is classified in dependence of the applied frequency and amplitude, so called large or small amplitude oscillatory rheology (LAOS - SAOS). In this context it is interesting to state that the energy dissipation scales equally with frequency and with amplitude. However it does not seem to be possible to reduce the measurement to energy dissipation or regimes of angular velocity [49, 50] since different material behaviours may be elucidated in dependence of the exact set of frequency and amplitude.

To give an example in figure 3.7 a response of mechanical stress and strain is illustrated for our model solution (described in section 3.8). The data corresponds to the LAOS behaviour of 30 % P123 diluted in heavy water for 1Hz and 5000 %. By looking at figure 3.7, it is apparent that the shape of the response function, mechanical stress σ clearly does not satisfy the shape of a sinus as stated in equation 3.4 as is expected for viscoelastic materials. Therefore the focus needs to be put on effects that are not explained by generalized Maxwell behaviour in the bulk. Generally, such departures from the expected behaviour are brought into context with flow instabilities and either the formation of shear bands or surface slip. Alternatively, also structural reorganisation of the bulk sample could be considered.

3.5 Break of mechanical continuum

In equation 3.1 the material is treated as a continuum and all modelling refers to the response as a property of the bulk. For certain complex fluids if sufficiently high shear is applied, the sample may get inhomogeneous and all the deformation will be dissipated in another structure that has different viscous properties, so called shear bands. This means effectively that the mechanical continuum between the surfaces is broken in different regions and that new

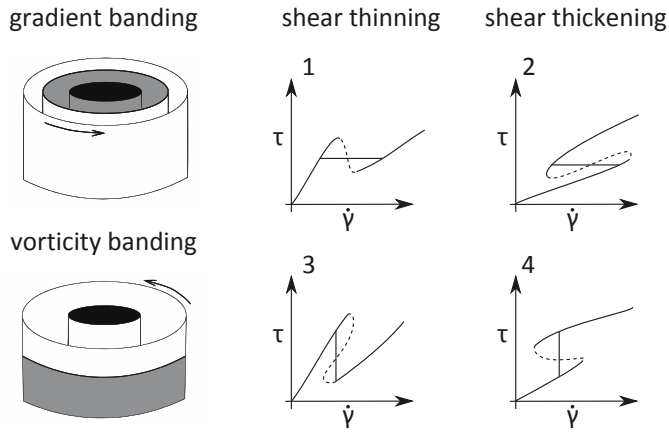

Figure 3.4. Reconstructed from [53]. The two different forms of shear banding are displayed and corresponding flow curves are depicted. Note that vorticity banding and shear thickening in the band structure are very rare, individually. In practice almost always behaviour 1, shear thinning in gradient banding, is observable, which was investigated in this thesis as well.

constitutive equations are needed to amend for this behaviour [51]. Two different forms of shear banding can be observed. A change of the properties along the shear gradient direction is called gradient banding and more rarely vortex bands, where the viscous properties differ along the vortex direction. A visualization of vorticity and gradient bands in direction of shear is depicted in figure 3.4, which is set in context to the data presented for our later described model solution in figure 3.10. For experimental visualization of shear bands, we refer to the reviews of Gurnon [52] and Olmsted [53].

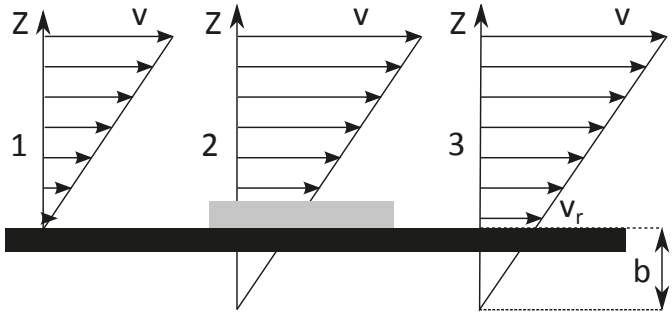

Figure 3.5. Reconstructed from [54]. Panel 1 shows the no slip hypothesis. The 2nd panel shows the death layer model (apparent slip) and in panel 3 real slip is displayed and the slip-length b is visualized.

3.6 Surface slip

In the 18th century, Bernoulli assumed for a liquid flowing through a pipe that the velocity of the cylinder must be the same as the liquid on it's surface [55]. This assumption was also made by Stokes [56]. This lead to the no surface slip boundary condition, which in case of wear, contradicts the natural observation. This is visualized in panel 1 from figure 3.5. Panel 2 shows the theory of a stagnant layer, called apparent slip. The extrapolation to a zero value is defined as the slip length b and was proposed by Navier and is illustrated in panel 3.

For all rheological considerations, the interplay between surface slip and roughness is important. It is crucial to mention that slip does not affect the viscosity, but the measurement of it. Generally all measurements of rheological properties are subdue to this influence. One of the few ways to remotely access the mechanism of this interplay is surface near scattering.

The importance of surface slip is illustrated by Escherichia coli bacteria swimming upstream by exploiting the boundary conditions [57], which is important in case of infection pathways. For a more detailed overview it is referred to the review article of Neto [54].

It is worth mentioning that neutron reflectivity and GISANS are one of the few methods available that can show how slip layers morphologically change in contrast to the bulk and therefore distinguish between apparent and real slip.

3.7 Probing rheology properties

> I had to retool myself as rapidly as possible.
>
> Douglas Hofstadter

This section provides a short overview of the used instruments for the investigation of complex fluids. Particular emphasis is put on the in-situ rheological studies with neutrons.

3.7.1 Rheometers

The first rheometer was the 1890s Ostwaldviskosimeter (a U-tube viscometer). The whole field started to be technically exploited after the invention of a falling ball viscosimeter by 1932 Fritz Hoeppler and was taken as a testing norm DIN-53655. A picture is displayed in figure 3.6. Both of these types just measured the absolute value of the viscosity under repeatable but non-tuneable conditions.
In the 1960s rheometers were developed, that focused on rotational geometries. Modern rheometers like the Anton Paar Physica MCR 501 or the TA Instru-

Figure 3.6. 1932 Fallkugelviskosimeter - falling ball viscosimeter on the left side and on the right side a modern rheometer with Couette cell (Anton Paar Physica MCR 501) mounted on the SANS beamline in Munich, FRM II, Germany.

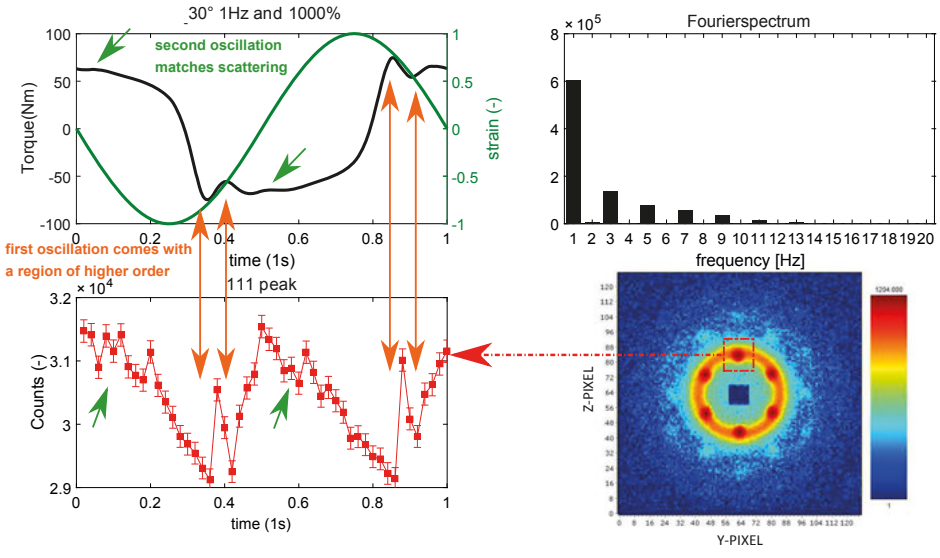

Figure 3.7. Experimental data of an aqueous solution of P123 under LAOS probed with Rheo-SANS. As clearly recognizable the black curve (upper right panel) is not a sinusoid. The intensity of the first order Bragg peak is put in relation to the waveform. A Fourier analysis is given to complement this information.

ments ARES use Couette (see figure 3.8) or cone plate geometry (as illustrated in 3.9) to access the properties of liquids. For cone plate geometry, the opening angle of the cone is chosen to apply a constant shear rate over the liquid. If a lot of sample with low viscosity is available, Couette geometry is supposed to provide more homogeneous loading, whereas for highly viscous substances, just cone plate geometry can be used to provide the necessary load. Naturally, cone plate geometry is chosen, if the amount of sample is limited. As with all machines, two different modes of energy release can be distinguished. Either the energy release is controlled over stress/torque or over strain/displacement of the motor. For the different aspects in this context, we refer to the work of Hans Läuger [58].

It is important to mention, that all rheological measurements are subject to the influence of surface slip and, therefore, of surface roughness, hence measures (e.g. standardized surfaces, gap scans, or a sufficient amount of sample) are taken to choose a modus operandi assuring this influence to be as minimal as possible.

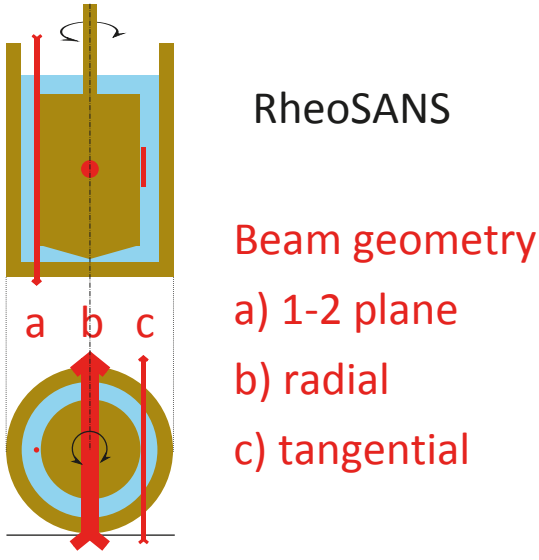

Figure 3.8. A display of the three different directions to be probed in terms of Couette geometry. It is possible to vary the beam over the gap in the 1-2 geometry and tangential geometry, whereas the resolution can be typically lowered in radial geometry [65]. The chassis and instrument head indicated in beige are supposed to be transparent to neutrons (like TiZr or Aluminium). The gap was made too big for illustration issues.

3.7.2 RheoSANS

RheoSANS is applying SANS (as described in section 2.3.1) but on a liquid under load in the geometries as displayed in figure 3.6 [59]. In this versatile technique it is crucial in what direction the shear gradient is in relation to the beam direction (as illustrated in 3.8). Even experiments normal to the flow direction (1-2 direction) can be probed [60] by a 1-2 shear cell [61], which enables direct access to shear bands. Other groups study mirco-fluidic behaviour [62]. RheoSANS requires the parts of the sample cell to be transparent to Neutrons (as described in 2.1.5) and typically null matrix materials such as aluminum or TiZR are used. To have material that is additionally transparent to light, quartz glass is used. This technique provides insight into how the bulk properties of liquids behave under shear and in light of anisotropy, making it possible to relate between the viscosity and the local structure on the length scales of the molecules or inter-atomic distances. One example of a LAOS cycles study for a micellar solution is given by Lopez-Barron [63]. For a complete discussion of rheoSANS we refer to the review of Aaron Eberle [64].
In paper III in a RheoSANS sample-cell straining of polymer-chains for certain shearing conditions was displayed.

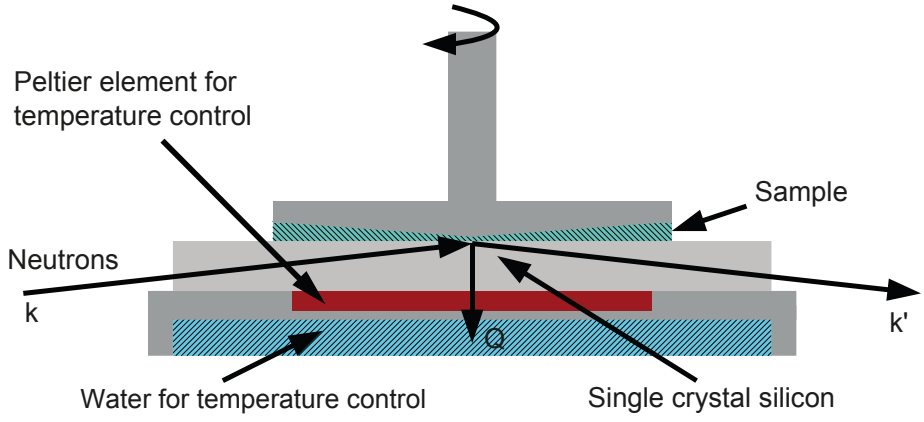

Figure 3.9. Typical geometry used for inter-facial neutron scattering studies combining load on a liquid [68][67]. The reflectivity signal is extracted by measuring systematically the intensity for wave-vectors k and k' that are traduced to the surface over the silicon block. The opening angle of the cone is chosen, so that the stress is uniform over a whole sheared area. Note that this requires horizontal geometry for the liquid not to leave the measurement gap. Reprint with the kind permission of the publisher (IUCR).

3.7.3 Rheo-Reflectivity

Using transparent materials to traduce neutrons to a surface of a liquid under load is called Rheo-Reflectivity as an effective combination of reflectivity measurements (as introduced in 2.2) by using a neutron transparent material like aluminium, quartz or silicon and cone-plate rheology. This is a way to directly probe interfaces and observe how the structure of a liquid changes under load in the vicinity of a surface. The pioneer-work done by Bill Hamilton to investigate the shear induced behaviour of an ionic viscoelastic fluid (CTAB in D20) under flow [26] was consequently followed by studies on surface ordering of micelles [66]. This was combined with an actual measuring tool for the investigation of interfaces under load [67]. The role of interfaces under shear can be investigated. In this context, it is for example possible to directly distinguish between apparent and real slip as displayed in figure 3.5. A visualization of the typical set-up is depicted in figure 3.9.

Paper II describes a time resolved Rheo-Reflectivity measurement of an aqueous solution of F127 under load. and Paper V describes the collapse of a polymer brush layer under shear load.

3.8 Sample properties and preparation

The samples investigated in this thesis are so called Pluronics, tri-block co polymers of EO - ethylene oxide and PO- propylene oxide that where dissolved in heavy water.

F127 (EO_{99}-PO_{65}-EO_{99}) is a linear triblock co-polymer a with a nominal molecular weight of 12600 g/mol and a weight fraction of PEO of approximately 70 % [69]. As visible from the structure of the polymer the core shows hydrophobic and the tails hydrophilic behaviour. This explains why above a critical temperature and above reaching a certain concentration in water micelles are formed. In this context the terms critical micellar concentration (cmc) and critical micellar temperature (cmt) are used. The structure of the polymer micelles and crystals formed by them was studied by Kell Mortensen at rest and under shear [70] and the bulk properties of this material are known [71]. In addition these micellar solutions have proven to be very sensitive to shear. Therefore they are used widely as industrial lubricant, as pharmacological drug delivery agent and in the chemical technical industry [72, 73]. In the presented study we use a model set-up being described in [67] and a model solution that is as aforementioned sensitive to shear [70]. A few complementary experiments were performed with P123 (EO_{20}-PO_{70}-EO_{20}) in 70 % heavy water, this solution has comparable properties.

A flow curve of F127 diluted in heavy water is given in figure 3.10. Notice the little buckle that indicates a break in mechanical continuum in accordance to the aforementioned gradient shear binning.

What was for the benefit of the experiment is that the solution shows a rich scattering behaviour due to the large SLD contrast by the usage of heavy water as solvent. The scattering length density b_{coh} of the heavy water is 6.381 10^{-6} $Å^{-2}$ and for the polymer 5.051 10^{-7} $Å^{-2}$, so the contrast provides an ample signal.

The interfacial scattering properties of this material are well investigated [65, 67, 69, 74, 75, 74] and the inter-facial scattering properties under oscillatory shear are exploited in paper II [68].

To prepare the sample advantage of the special phase behaviour illustrated in figure 3.11, that it melts when cooled, was taken and the blending was performed in fridges at 10 degrees Celsius, since then the polymer is solvable in water without building flocks immediately.

Gratitude to Mrs. Adelman (sic) from BASF America for providing an ample supply.

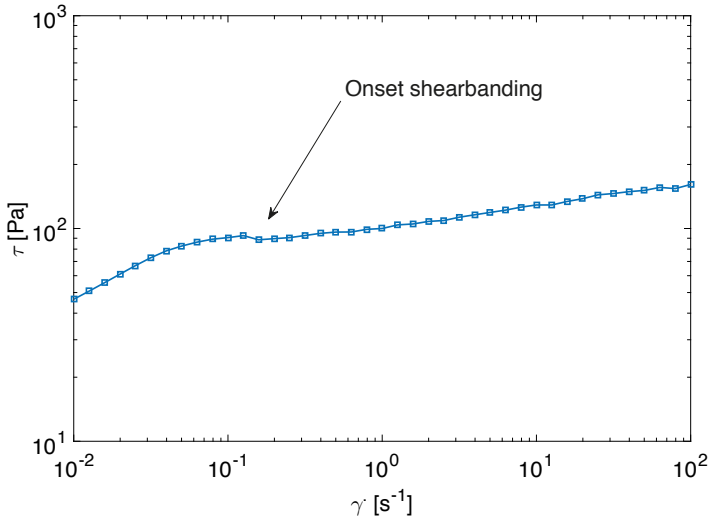

Figure 3.10. Flow curve (shear stress over shear rate) of F127 measured in Couette geometry on an Anton Paar MCR 501 rheometer. Notice the same behaviour as in figure 3.4 inlay 1. The marked jump toward can not be explained without discontinuity and is therefore a strong indicator for shear banding.

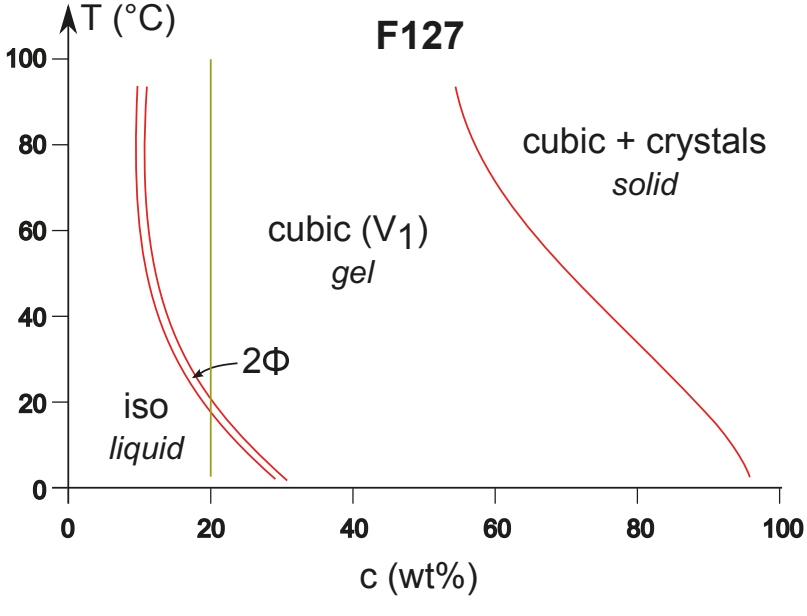

Figure 3.11. Phase diagram of F127 dissolved in water. The concentration that was used is displayed with the moss-green line [71]. Interestingly the substance melts while cooled. Reprint with the kind permission of the publisher (IUCR)

4. Presented papers and outlook

> Quod fuit, ipsum est, quod futurum est. Quod factum est, ipsum est, quod faciendum est: nihil sub sole novum.
>
> Ecclesiastes 1:9

After surface orientation studies in micelles began 30 years ago, further aspects of the connection between interfaces and mechanical load have been investigated in this thesis. In this context mainly three different projects have been finalized.

4.1 GISANS and penetration depth variation

GISANS with a limited resolution was applied on F127 in heavy water solution to unveil the lateral ordering of the liquids on interfaces. By varying the wavelength, information on the surface near structure could be extracted as seen in Paper I [74]. In this study, an out of plane feature was discovered in a region where evanescent scattering is to be expected. We concluded that this bias is due to resolution effects. In Paper VI [76] consequently a method was developed to estimate the influence of resolution functions on the penetration depth. This information is used to recover depth resolution, similar to tomography. A statistical analysis of the penetration depth was performed.

4.2 Stroboscopic inter-facial scattering

Scattering experiments were successfully conducted and a surface order in micellar solutions over the LAOS cycle was classified. To realize this, software for stroboscopic experiments has been developed and is presented in Paper II [68]. In this context, a technique for linking the neutron events to the excitation of a waveform in order to reintegrate the scattering data, is developed and presented. Neutron reflectivity data on a micro second time scale is presented for the first time. The normalization of stroboscopic experiments is discussed especially in the context of low pulse spallation sources and the implications for normalization was investigated in Paper VII. In the presented two papers,

the underlying theoretical and technical aspects of stroboscopic experiments were illustrated. From this a methodology to investigate related phenomena was developed. Complementary in Paper V a simulation tool for polymer brushes that occurs under load is presented, which is compared with neutron reflectivity data of PS in DEP on a PS brush under shear [77].

4.3 New methods for instrumentation

In Paper III a shearing apparatus that operates without inducing magnetic fields, meaning to be entirely made of aluminium and driven by pressured air, was developed. NSE (Neutron spin echo) data was collected of a highly entangled polymer [78].

An algorithm to efficiently transform data to momentum transfer space from instrument space, for monochromatic and time of flight instruments alike, was developed and a free standing software package corresponding to the problem is presented in paper IV [34]. This enables the possibility of using two dimensional position sensitive detectors.

In the context of stroboscopic reintegration the many advantages of GPS time stamped event mode data became apparent. Including all kinds of instrument values (e.g. temperature, humidity, moderator temperature etc.) with an appropriate sampling frequency as non neutron events, makes data mining and sample observation in the post processing feasible.

4.4 Outlook

With new accelerator based sources upcoming, the normalization effects become far more important than in the past with monochromatic and relatively stable reactor sources. Especially with higher flux instruments and long pulses new experiments investigating similar questions will be conducted. For these types of experiments parts of this work will be critical. This shall be put in context that new dedicated TOF general purpose instruments should be built offering GISANS opportunities in combination with horizontal geometry similar to PLATYPUS @ ANSTO.

Generally, all papers describe a new attempt to overcome limits in instrumentation or new software to illustrate corresponding problems. The main result of the thesis is that the needs of instrumentation for the investigation of effects in complex fluids have been identified and possible solutions have been developed.

Altogether the presented paper containing the thesis can be seen as a cost effective and easy augmentation for existing instruments.

5. Populärvetenskaplig sammanfattning

Jag är en tvivelaktig figur
duger ej mycket till.
Bakom ett hörn står döden på lur,
han tar mig när han vill.

Cornelis Vreeswijk

Förståelsen av hur komplexa vätskor uppför sig är av stor betydelse. Dessa vätskor förekommer både i naturen - biologiskt sett (t.ex. blod vid kärlväggar) och i tekniska anläggningar inom exempelvis plastindustrin.

I detta sammanhang är en komplex vätska av den sorten att dess uppförande förändras i förhållande till den belastningen den utsätts för och att vätskan ofta har egenskaper av både fast och flytande tillstånd - som exempelvis honung. Sådana egenskaper uppstår när materialets interna tidsspann ligger inom samma ram vad gäller tid som människans förmåga att åskåda . På liknande sätt flöder glas i årtusenden ner till marken, såsom det går att beskåda i gamla kyrkor.

Särskild betydelse får detta vid de gränsytor där alla interaktioner i livet sker på ytan. Detta kan exempelvis illustreras av gummidäck - om man ställer in den interna friktionen av materialet till att vara i samklang med ytans friktion.

Att införskaffa en djupgående förståelse av samspelet mellan mikrostrukturer, vätskor och ytreaktioner är målet för många ansträgningar inom forskning. Ett målande och för Sverige typiskt exempel - att åka skridskor - går att se i bild 5.1. För att åstadkomma detta användes här neutronspridningstekniker för att iaktta egenskaper hos komplexa vätskor utsatta för belastning. Neutroner erbjuder en utomordentlig möjlighet att undersöka gränsytan mellan fast och flytande form, eftersom många material blir transparenta vid neutronstrålning och neutronerna interagerar med de inblandade ämnenas atomkärnor.

Neutronerna produceras i en så kallad neutronkälla, antingen genom kärnfission i en forskningsreaktor eller genom spallation (en tungmetalls atomkärnor destabiliseras och avger neutroner efter att ha bestrålats med protoner) i en specialiserad partikelaccelerator. Slutlingen analyseras neutronerna av mätinstrument. Arbetat har huvudsaklingen bestått av att vidareutveckla och förfina tekniken av de mätinstrument som har använts. Med hjälp av ett speciellt kemiskt modellsystem och en reometer (en maskin som mäter flytförhållandet av skjuvade vätskor) kunde gränsskiten utforskas under kontrollerad belastning.

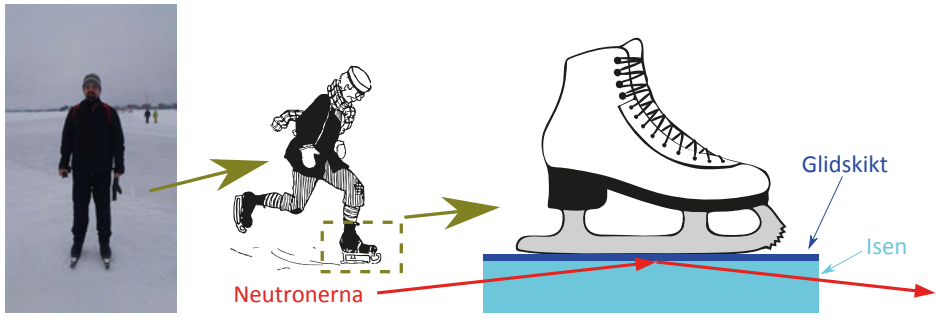

Figure 5.1. Genom att titta på anledningen till varför författaren valde att komma till Sverige kan man illustrera betydelsen av att undersöka fasta- och flytande gränsytar under belastning. Att åka skridskor fungerar bara bra om det bildas en glidskikt. Under vilka omständigheter dessa skikt bildas bestod under en lång tid av spekulationer och felsökningar. I motsats till skidåkning spelar den mekaniska belastningen ingen roll, vilket slutligen bevisades genom spridningsexperiment.

I detta sammanhang var det möjligt att visa både yt- och materialreaktioner under cyklisk påfrestning, såsom de förekommer i typiska maskindelar, och därmed fastställa kopplingen mellan mikroskopiska förändringar och makroskopisk belastning.

Ytterligare utvecklades en djupkänslig metod för att lösa upp den vågrätt liggande strukturen hos en vätska som befinner sig vid gränskiktet. I detta sammanhang utvecklades också en algoritm för att informationen från de vetenskapliga instrumenten bättre ska kunna representeras.

6. Populärwissenschaftliche Zusammenfassung

> Grau, teurer Freund, ist alle
> Theorie // Und grün des Lebens
> goldner Baum.
>
> Mephistopheles

Das Verständnis des Verhaltens von komplexen Flüssigkeiten ist von enormen Bedeutung. Diese kommen in der Natur häufig vor, sowohl in biologischer Hinsicht (Blut an Gefässwänden) als auch in technischen Anlagen, wie zum Beispiel in der Kunststoffindustrie.

Eine komplexe Flüssigkeit ist in diesem Zusammenhang eine Flüssigkeit die ihr Verhalten in Abhängigkeit der Belastung verändert und oft Eigenschaften hat die zwischen einem Festkörper und einer Flüssigkeit liegen, wie zum Beispiel Honig. Solche Eigenschaften kommen zu stande, wenn die internen Zeiträume des Materials im selben Rahmen wie die Beobachtungszeiträume des Menschen liegen. So läuft Glas etwa in Jahrtausenden zu Boden, wie man in alten Kirchen beobachten kann.

Besondere Bedeutung kommt den Grenzflächen zu, da alle Interaktionen im Leben über Oberflächen vonstatten gehen. Dies kann an Gummireifen veranschaulicht werden, wenn man die interne Reibung des Materials im Einklang mit der Reibung an der Grenzfläche einstellt.

Ein tiefgreifendes Verständnis des Zusammenspiels der Mikrostruktur mit den Fliesseigenschaften und den Oberflächenreaktionen ist deshalb Gegenstand zahlreicher Forschungsunternehmungen. Ein anschauliches und für Schweden typisches Beispiel, das Eislaufen, sieht man in Bild 6.1.

Um dies zu verwirklichen wurden in dieser Arbeit Neutronenstreutechniken angewandt um das Verhalten von komplexen Flüssigkeiten unter Last zu beobachten. Neutronen sind eine wesentliche Möglichkeit um Flüssig - Fest Grenzflächen zu untersuchen, da viele Materialien transparent zu Neutronenstrahlung sind und Neutronen mit den Atomkernen der beteiligten Elemente interagieren.

Die Neutronen werden in einer sogenannten Neutronenquelle, durch Kernspaltung an einem Forschungsreaktor oder durch Abspaltung (ein Protonenstrahl trifft auf ein Schwermetall und zerstört den Kern) an einem darauf spezialisierten Teilchenbeschleuniger produziert und dann an speziell darauf angepassten Messinstrumenten analysiert. Der Hauptteil des Werkes lag auf der Weiterentwicklung und Verfeinerung der an diesen Messinstrumenten eingesetzten Techniken.

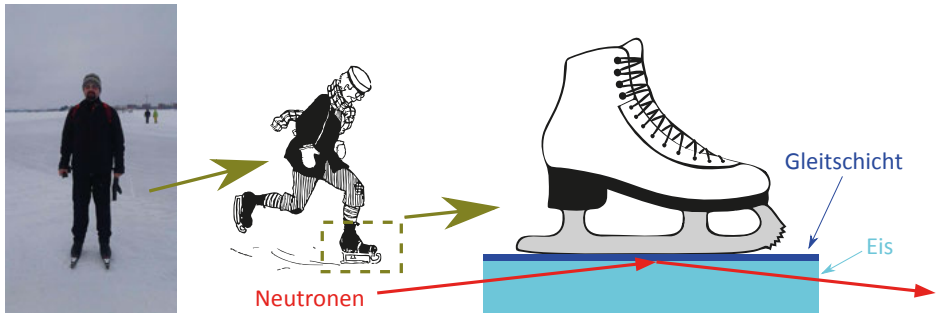

Figure 6.1. Man sieht am Grund, weshalb der Author nach Schweden kam, die Bedeutung der Untersuchung von Fest - Flüssig Grenzflächen unter Last. Das Schlittschuhefahren geht nur gut, wenn sich eine Gleitschicht bildet. Unter welchen Bedingungen sich diese bildet war lange Zeit Teil von Spekulationen und Irrwegen. Dass im Gegensatz zum Schifahren die mechanische Belastung dabei keine Rolle spielt, wurde letztlich durch Streuexperimente gezeigt.

Wir konnten mit einem speziellen Modellsystem diese Grenzfläche untersuchen und mit einem Rheometer, einer Maschine die das Fliessverhalten von gescherten Flüssigkeiten misst, kontrolliert Lasten aussetzen. In diesem Kontext war es möglich sowohl Oberflächen- als auch Materialreaktionen in Abhängigkeit einer zyklischen Belastung, wie sie in typischen Maschinenteilen vorkommt, zu zeigen und damit eine Verbindung zwischen mikroskopischen Veränderung und makroskopischen Belastungen herstellen.

Zusätzlich wurde eine Methode entwickelt um die waagrecht liegende Struktur von einer Flüssigkeit an der Grenzfläche in der Tiefe aufzulösen. In diesem Zusammenhang wurde auch ein Algorithmus entwickelt um die Daten der wissenschaftlichen Instrumente besser darzustellen.

7. Acknowledgements / Dedications

Sine ira et studio.

Publius Cornelius Tacitus

First of all I have to thank my supervisor Max Wolff, who employed me initially, opened the gates to the exciting world of neutrons, provided the academic freedom to make this work possible and guided me patiently through the very dysfunctional world of academia.

A big place in the thesis has the team from the SNS, Oak Ridge National Laboratory, Tennessee, USA; John Francis Ankner, Jim Browning, Candice Elizabeth Halbert, Bogdan Vacaliuc, Andre Parizzi, Jean Chrisophe Bilheux, David Uhrig and Brad Lokitz, who helped me getting my PHD started, did not leave me alone at the physically straining beam times and subsequently contributed substantially to the scientific cases of all my work. Without you it would not have been possible!

A special thanks is to my two students Maciej Kawecki and Jörg Herbel, both whose work came to fruition in publication.

For my friend Airidas Korolkovas from the University of Uppsala for being an inspiration in the scientific community.

I want to express my gratitude to Sebastian Busch from the research reactor in Munich, BRD, who competently supported me during a difficult beam-time in a very difficult time of my life.

To my friend Brian Kitchen from the University of Uppsala who provided (and provides) an example how to lead life.

Einen Platz hier hat auch Sara Persson, die mir geholfen hat die schwedische Zusammenfassung zu erstellen.

A great thanks is to pixabay, wikipedia, Inkscape and creative commons, that deployed free to use (vector-)graphics to put together the illustrations..

The free fruits and the tea was very appreciated at Ångströms. That really helped me every day to get started. I hope I did not accidentally took from the

chemistry department too many times.

For Gunnar K. Palsson, Tobias Warnatz, Andreas Bliersbach, Andreas Frisk and Emil Melander for including me in memorable social happenings.

Thanks to the Liljevalch foundation to grant me travel stipends to international conferences.

For my office colleagues Henry Stopfel and Sotirios Droulias, who accompanied and supported me during the whole time. Thank you for the refreshing discussions and the amicable atmosphere.

Jag vill uttrycka min tacksamhet till kungen och det svenska folket, som har finansierat min forskning och byggt upp ett beundransvärt samhälle, vilket de varit så generösa och snälla att låta mig delta i.

An dieser Stelle sei unseren Ahnen gedacht, die durch Ihre Schaffenskraft und Ihren Aufopferungswillen unser aller modernes Leben ermöglicht haben.

Till min sambo, Ylva Fahleson, som har berikat mitt liv och har öppnat dörrarna till den Svenska världen för mig.

Schlussendlich ist dieses Werk meiner Mutter gewidmet, die mich Zeit meines Lebens immer unterstützt hat.

Thank you for your help
Tack för all support
Danke für Eure Unterstützung,
Adlmann Franz Alois

8. References

[1] Jens Als-Nielsen and Des McMorrow. *Elements of Modern X-ray Physics*. Wiley, 2011.

[2] Peter S. Pershan and Mark L. Schlossmann. *Liquid Surfaces and Interfaces: Synchrotron X-ray Methods*. ISBN 978-0-521-81401-0. Cambridge University Press (CUP), The Edinburgh Building, Cambridge CB2 8RU, UK, 2012.

[3] V. F. Sears. Dynamical theory of neutron diffraction. *Canadian Journal of Physics*, 56:1261–1288, 1978.

[4] V. F. Sears. Theory of multilayer neutron monochromators. *Acta Cryst.*, A39:601–608, 1983.

[5] James Chadwick. Existence of a neutron. *Proceedings of the Royal Society A*, 136:692–708, 1932.

[6] J. R. Lamarsh and A. J. Baratta. *Introduction to nuclear engineering*, volume 3. Prentice Hall, 2001.

[7] E Fermi and W.H. Zinn. Reflection of neutrons on mirrors. *Oak Ridge, Tenn. : Manhattan District Declassified Code, Physical Review*, 70:101–103, 1946.

[8] Andrew Taylor, Mike Dunne, Steve Bennington, Stuart Ansell, Ian Gardner, Peter Norreys, Tim Broome, David Findlay, and Richard Nelmes. A route to the brightest possible neutron source? *Science*, 315:1092–1095, 2007.

[9] Jielong Su, Vikram S. Raghuwanshi, Warwick Raverty, Christopher J. Garvey, Peter J. Holden, Marie Gillon, Stephen A. Holt, Rico Tabor, Warren Batchelor, and Gil Garnier. Smooth deuterated cellulose films for the visualisation of adsorbed bio-macromolecules. *Scientific Reports*, 6:36119, 2016.

[10] Varley F. Sears. Neutron scattering lengths and cross sections. *Neutron News, Vol. 3, No. 3, 1992, pp. 29-37*, 3:29–37, 1992.

[11] Takuo Okuchi, Akinori Hoshikawa, and Toru Ishigaki. Forge-hardened tizr null-matrix alloy for neutron scattering under extreme conditions. *Metals*, 5:2340–2350, 2015.

[12] Q. Yang and L.R. Zhao. Characterization of nano-layered multilayer coatings using modified bragg law. *Materials Characterization*, 59(9):1285 – 1291, 2008.

[13] C. F. Majkrzak and N. F. Berk. Exact determination of the phase in neutron reflectometry. *Phys. Rev. B*, 52:10827, 1995.

[14] V.-O. de Haan, A. A. van Well, S. Adenwalla, and G. P. Felcher. Retrieval of phase information in neutron reflectometry. *PHYSICAL REVIEW B*, 52:10831, 1995.

[15] L.G. Parratt. Surface studies of solids by total reflection of x-rays. *Physical Review*, 95:359, 1954.

[16] F. Abeles. La theorie generale des couches minces. *Le Journal de Physique et le Radium*, 11:307–310, 1950.

[17] D.S. Sivia. *Elementary Scattering Theory*. Oxford University Press, 2011.

[18] Metin Tolan. *X-Ray Scattering from Soft-Matter Thin Films*. Springer-Verlag Berlin Heidelberg, 1999.

[19] M. Bjoerck and G. Andersson. Genx: an extensible x-ray reflectivity refinement program utilizing differential evolution. *Journal of Applied Crystallography*, 40(details):1174–1178, 2007.
[20] S.K. Sinha and H. Stanley. X-ray and neutron scattering from rough surfaces. *Phys. Rev. B*, 38:2297, 1988.
[21] L. Nevot and P. Croce. Caracerrisation des surfaces par reflexion rasante de rayons x. application a l etude du polissage de quelques verres silicates. *Revue de Physique Applique*, 15(3):761–779, 1980.
[22] Krassimir Stoev and Kenju Sakurai. Recent theoretical models in grazing incidence x-ray refiectometry. *The Rigaku Journal*, 14:22, 1997.
[23] Wim G. Bouwman and Jan Skov Pedersen. Resolution function for two-axis specular neutron refleetivity. *J.. Appl. Cryst.*, 29:152–158, 1996.
[24] Andrew Robert John Nelson. Towards a detailed resolution smearing kernel for time-of-flight neutron reflectometers. *J Appl Crystal*, 46(5):1338–1346, Sep 2013.
[25] J.R. Levine, J.B. Cohen, Y.W. Chung, and P. Georgopouls. Grazing-incidence small-angle x-ray scattering: New tool for studying thin film growth. *J. Appl. Cryst*, 22:528–532, 1989.
[26] W. A. Hamilton, P. D. Butler, S. M. Baker, G. S. Smith, John B. Hayter, L. J. Magid, and R. Pynn. Shear induced hexagonal ordering observed in an ionic viscoelastic fluid in flow past a surface. *Physical Review Letters*, 72:2219, 1994.
[27] W.A. Hamilton, P.D. Butler, John B. Hayter, L.J. Magid, and P.J. Kreke. Over the horizon sans. measurement on near surface poiseuille shear induced ordering of dilute solutions of threadlike micelles. *Physica B*, 221:309–319, 1996.
[28] Alexander Hexemer and Peter Muellller Buschbaum. Advanced grazing-incidence techniques for modern soft-matter materials analysis. *IUCrJ*, 2:106–125, 2015.
[29] B. Toperverg, H. Lauter, and Lauter V. Reflectivity off-specular scattering, and gi-sas: Neutrons.
[30] C. Durniak J. Burle, J. M. Fisher, M. Ganeva, G. Pospelov, W. Van Herck, and J. Wuttke. Bornagain - software for simulating and fitting x-ray and neutron small-angle scattering at grazing incidence , version 1.8, http://www.bornagainproject.org, 2017.
[31] Remi Lazzari. Isgisaxs: a program for grazing-incidence small-angle x-ray scattering analysis of supported islands. *J. Appl. Cryst.*, 35:406–421, 2002.
[32] S. V. Kozhevnikov and F. Ott. Representation of data on off-specular neutron scattering. *Phys. Solid State*, 52(8):1561–1570, Aug 2010.
[33] Fredric Ott and Sergey Kozhevnikov. Off-specular data representations in neutron reflectivity. *J Appl Cryst*, 44(2):359–369, Feb 2011.
[34] F. A. Adlmann, G. K. Palsson, J. C. Bilheux, J. F. Ankner, P. Gutfreund, M. Kawecki, and M. Wolff. Oeverlaotaren: a fast way to transfer and orthogonalize two-dimensional off-specular reflectivity data. *Journal of Applied Crystallography*, 49(6):2091–2099, Nov 2016.
[35] Robert Cubitt, Thomas Saerbeck, Richard A. Campbell, Robert Barker, and Philipp Gutfreund. An improved algorithm for reducing reflectometry data involving divergent beams or non-flat samples. *J. Appl. Cryst.*, 48:2006–2011, 2015.
[36] John F. Ankner. Absolute intensity normalization of a polychromatic neutron

beam. 2012.
[37] Peter Fratzl. Small-angle scattering in materials science - a short review of applications in alloys, ceramics and composite materials. *J. Appl. Cryst.*, 36:397, 2003.
[38] Jan Skov Pedersen. Analysis of small-angle scattering data from colloids and polymer solutions: Modeling and least-squares fitting. *Adv. Colloid Interface Sci.*, 70:171–210, 1997.
[39] R. M. Dalgliesh, Y. G. J. Lau, R. M. Richardson, and D. J. Riley. Millisecond time resolution neutron reflection from a nematic liquid crystal. *Review of Scientific Instruments*, 75(9):2955, 2004.
[40] A. Wiedenmann, U. Keiderling, K. Habicht, M. Russina, and R. Gaehler. Dynamics of field-induced ordering in magnetic colloids studied by new time-resolved small-angle neutron-scattering techniques. *Physical Review Letters*, 97(5), Aug 2006.
[41] D. Kipping, R. Gaehler, and K. Habicht. Small angle neutron scattering at very high time resolution: Principle and simulations of tisane. *Physics Letters A*, 372(10):1541–1546, Mar 2008.
[42] R. Callens and J. Odeurs. Principles of stroboscopic detection of nuclear forward-scattered synchrotron radiation. *Physical Review B*, 67:104423, 2003.
[43] www.nobelprize.org/nobel_prizes/physics/laureates/1991/press.html.
[44] P. G. de Gennes. Reptation of a polymer chain in the presence of fixed obstacles. *The Journal of Chemical Physics*, 55:572, 1971.
[45] Katherine M.N Oates, Wendy E Krause, Ronald L Jones, and Ralph H Colby. Rheopexy of synovial fluid and protein aggregation. *Journal of The Royal Society Interface*, 3(6):167–174, 2006.
[46] G. K. Batchelor. *An Introduction to Fluid Dynamics*. ISBN 0-521-66396-2. Cambridge University Press, 1967.
[47] Kzy Hyun, Manfred Wilhelm, Christopher O. Klein, Kwang Soo Cho, Jung Gun Nam, Kyung Hyun Ahn, Seung Jong Lee, Randy H. Ewoldt, and Gareth H. McKinley. A review of nonlinear oscillatory shear tests: Analysis and application of large amplitude oscillatory shear (laos). *Progress in Polymer Science*, 36:1697–1753, 2011.
[48] Michelle A. Calabrese, Norman J. Wagner, and Simon A. Rogers. An optimized protocol for the analysis of time-resolved elastic scattering experiments. *Soft Matter*, 12(8):2301–2308, 2016.
[49] K. Hyun, S. H. Kim, K. H. Ahn, and S. J. Lee. Large amplitude oscillatory shear as a way to and classify the complex fluids. *J. Non-Newtonian Fluid Mech.*, 107:51 – 65, 2002.
[50] Simon A. Rogers and M. Paul Lettinga. A sequence of physical processes determined and quantified in large-amplitude oscillatory shear (laos): Application to theoretical nonlinear models. *J. Rheol.*, 56(1):1, 2012.
[51] M.A. Fardin, T.J. Ober, C. Gay, G. Gregoire, G.H. McKinley, and S. Lerouge. Potential ways of thinking about the shear banding phenomenon. *Soft Matter*, 7, 2011.
[52] A. Kate Gurnon, Carlos Lopez-Barron, Matthew J. Wasbrough, Lionel Porcar, and Norman J. Wagner. Spatially resolved concentration and segmental flow alignment in a shear-banding solution of polymer-like micelles. *ACS Macro Lett.*,

3:276–280, 2014.
[53] Peter D. Olmsted. Perspectives on shear banding in complex fluids. *Rheologica Acta*, 47(3):283–300, Apr 2008.
[54] Chiara Neto, Drew R Evans, Elmar Bonaccurso, Hans-Juergen Butt, and Vincent S J Craig. Boundary slip in newtonian liquids: a review of experimental studies. *Rep. Prog. Phys.*, 68:2859–2897, 2005.
[55] Daniel Bernoulli. *Hydrodynamica*. Typographi Bafilienfis, 1738.
[56] George Gabriel Stokes. On the theories of the internal friction of fluids in motion and of the equilibrium and motion of elastic solids. *Trans. Cambridge Philos. Soc.*, 8:287–319, 1845.
[57] Jane Hill, Ozge Kalkanci, Jonathan L. McMurry, and Hur Koser. Hydrodynamic surface and interactions enable and escherichia coli and to seek and efficient routes and to swim and upstream. *Physical Review Letters*, 98:068101, 2007.
[58] Jörg Läuger and Heiko Stettin. Differences between stress and strain control in the non-linear behavior of complex fluids. *Rheol Acta*, 49:909–930, 2010.
[59] Aaron P. R. Eberle, Paul D. Butler, Carlos R. Lopez-Barron, A. Kate Gurnon, Norman J. Wagner, and Lionel Porcar. State of the art tools to investigate soft matter under flow. 2014.
[60] Matthew Liberatore, Florian Nettesheim, Norman Wagner, and Lionel Porcar. Spatially resolved small-angle neutron scattering in the 1-2 plane: A study of shear-induced phase-separating wormlike micelles. *Phys. Rev. E*, 73(2), Feb 2006.
[61] A. Kate Gurnon, P. Douglas Godfrin, Norman J. Wagner, Aaron P. R. Eberle, Paul Butler, and Lionel Porcar. Measuring material microstructure under flow using 1-2 plane flow-small angle neutron scattering. *JoVE*, (84), 2014.
[62] Carlos G. Lopez, Takaichi Watanabe, Anne Martel, Lionel Porcar, and Joao T. Cabral. Microfluidic-sans: flow processing of complex fluids. *Scientific Reports*, 5:7727, 2015.
[63] Carlos R. López-Barrón, Lionel Porcar, Aaron P. R. Eberle, and Norman J. Wagner. Dynamics of melting and recrystallization in a polymeric micellar crystal subjected to large amplitude oscillatory shear flow. *Physical Review Letters*, 108:258301, 2012.
[64] A. P. R. Eberle and L. Porcar. Flow-sans and rheo sans applied to soft matter. *Current Opinion in Colloid & Interface Science*, 17:33–43, 2012.
[65] Jun Jiang, Christian Burger, Chunhua Li, Jun Li, Min Y. Lin, Ralph H. Colby, Miriam H. Rafailovich, and Jonathan C. Sokolov. Shear-induced layered structure of polymeric micelles by sans. *Macromolecules*, 40(11):4016–4022, May 2007.
[66] Max Wolff, Uwe Scholz, Rainer Hock, Andreas Magerl, Vincent Leiner, and Hartmut Zabel. Crystallization of micelles at chemically terminated interfaces. *Physical Review Letters*, 92:255501, 2004.
[67] M. Wolff, P. Kuhns, G. Liesche, J. F. Ankner, J. F. Browning, and P. Gutfreund. Combined neutron reflectometry and rheology. *Journal of Applied Crystallography*, 46:17291733, 2013.
[68] F. A. Adlmann, P. Gutfreund, J. F. Ankner, J. Browning, A. Parizzi, B. Vacaliuc, C. E. Halbert, J.P. Rich, A. J. C. Dennison, and M. Wolff. Towards neutron scattering experiments with sub-millisecond time resolution. *Journal of Applied Cr*, 48(1):220–226, February 2015.

[69] Kyu Hyun, Jung Gun Nam, Manfred Wilhellm, Kyung Hyun Ahn, and Seung Jong Lee. Large amplitude oscillatory shear behavior of peo-ppo-peo triblock copolymer solutions. *Rheologica Acta*, 45(3):239–249, Jan 2006.

[70] Kell Mortensen. Structural studies of aqueous solutions of peo-ppo-peo and triblock copolymers and their micellar aggregates and and mesophases; a small-angle neutron scattering study. *J. Phys.: Condens. Matter 8*, 8:A103–A124, 1996.

[71] G. Wanka, H. Hoffman, and W. Ulbricht. Phase diagrams and aggregation behavior of poly(oxyethylene)-poly(oxypropylene)-poly(oxyethylene) triblock copolymers in aqueous solutions. *Macromolecules*, 27:4145–4159, 1994.

[72] Gilles Dumortier, Jean Louis Grossiord, Florence Agnely, and Jean Claude Chaumeil. A review of poloxamer 407 pharmaceutical and pharmacological characteristics. *Pharmaceutical Research*, 23(12):2709–2728, Nov 2006.

[73] Ezra Feilden. Robocasting of structural ceramic parts with hydrogel inks. *Journal of the European Ceramic Society*, 10:2525–2533, 2016.

[74] M. Wolff, J. Herbel, F. Adlmann, A. J. C. Dennison, G. Liesche, P. Gutfreund, and S. Rogers. Depth-resolved grazing-incidence time-of-flight neutron scattering from a solid-liquid interface. *Journal of Applied Crystallography*, 47:130–135, 2014.

[75] M. Wolff, A. Magerl, and H. Zabel. Structure of polymer micelles close to the solid interface. *The European Physical Journal E*, 16(2):141 145, Feb 2005.

[76] Franz A Adlmann, Joerg Herbel, Airidas Korolkovas, Andreas Bliersbach, Boris Toperverg, Walter Van Herck, Gunnar K Palsson, Brian Kitchen, and Max Wolff. Depth resolved grazing incidence neutron scattering experiments from semi-infinite interfaces: a statistical analysis of the scattering contributions. *J. Phys.: Condens. Matter*, 30:165901, 2018.

[77] Airidas Korolkovas, Cesar Rodriguez-Emmenegger, Andres de los Santos Pereira, Alexis Chennevire, Frederic Restagno, Maximilian Wolff, Franz A. Adlmann, Andrew J. C. Dennison, and Philipp Gutfreund. Polymer brush collapse under shear flow. *Macromolecules*, 50(3):1215–1224, Feb 2017.

[78] M. Kawecki, P. Gutfreund, F. A. Adlmann, E. Lindholm, S. Longeville, A. Lapp, and M. Wolff. Probing the dynamics of high-viscosity entangled polymers under shear using neutron spin echo spectroscopy. *Journal of Physics: Conference Series*, 746:012014, 2016.

Acta Universitatis Upsaliensis

Digital Comprehensive Summaries of Uppsala Dissertations from the Faculty of Science and Technology 1666

Editor: The Dean of the Faculty of Science and Technology

A doctoral dissertation from the Faculty of Science and Technology, Uppsala University, is usually a summary of a number of papers. A few copies of the complete dissertation are kept at major Swedish research libraries, while the summary alone is distributed internationally through the series Digital Comprehensive Summaries of Uppsala Dissertations from the Faculty of Science and Technology. (Prior to January, 2005, the series was published under the title "Comprehensive Summaries of Uppsala Dissertations from the Faculty of Science and Technology".)

Distribution: publications.uu.se
urn:nbn:se:uu:diva-348348

ACTA
UNIVERSITATIS
UPSALIENSIS
UPPSALA
2018